THE DESIGN OF AN IN-CONDUIT HYDROPOWER PLANT WITH A SEAL-FREE MAGNETIC TRANSMISSION

by

Casey Lloyd Nichols

A thesis submitted to the faculty of
The University of North Carolina at Charlotte
in partial fulfillment of the requirements
for the degree of Master of Science in
Applied Energy and Electromechanical Systems

Charlotte

2019

Approved by:

____
Dr. Wesley B. Williams

____
Dr. Joshua A. Tarbutton

____
Dr. Rodward L. Hewlin Jr.

ABSTRACT

CASEY LLOYD NICHOLS. The Design of a Hydropower Plant with a Seal-free Magnetic Transmission. (Under the direction of DR. WESLEY B. WILLIAMS)

Presently, governments are focused on the development of diverse energy sources from renewable supplies. A major part of that is the development of pico-hydro and micro-hydro power generation in low head, low flow rate rivers and streams. Numerous dams have been identified that currently lack power generation features even though there is potential to produce energy. There is a need for innovative hydropower plants that are simple to install and reliable. This novel design of a magnetic transmission reaction turbine (MTRT) hydropower plant uses a contact-free, magnetic transmission to eliminate the need for mechanical seals. The removal of the sealing component creates a more robust design that has the potential to decrease maintenance cost and increase efficiency subsequently decreasing the levelized cost of energy. The use of a magnetic transmission in this design eliminates the need for mechanical seals which inherently add friction and have a limited life. With the use of permanent magnets attached to the reaction turbine rotor within a conduit, the rotational energy of the turbine can be transmitted through the pipe walls with magnetic forces into the rotating outer rotor which is part of a belt-pulley speed increase. The increased rotational speed in the high-speed shaft is connected to a generator for power generation. The nature of the design is modular in that it is intended to be installed where current dams exist with as few modifications as possible. This research will begin to develop a product that offers a solution for the current market's need for low cost, low maintenance, hydropower plants. This thesis is brought forward to describe and document the novel design.

ACKNOWLEDGEMENTS

I would like to thank everyone who supported my research and my progression through this master's degree. Firstly, I would like to thank my professor, principal investigator, committee chair and friend, Dr. Wesley Williams for his patience, motivation, and immense knowledge that was necessary for the completion of this research. I owe the success of this thesis to his mentorship and unwavering support. I would also like to thank the other members of my committee, Dr. Rodward Hewlin Jr. and Dr. Joshua Tarbutton, for their support and membership on my thesis committee. I would also like to thank my mother, father and sister for their continued support through my life and academic career. I would also like to thank my co-workers and friends Sina Modaresahmadi, David Barnett, Dr. Kang Li, Austin Joyner and Ryan Williams for their help and camaraderie through my undergraduate and graduate degrees. I would also like to thank my dog Miss Betsy for her friendship through this research.

Thank you to the UNC Coastal Studies Institute for funding the magnetic gearing research group at UNC Charlotte and my graduate research assistantship. Thank you to the UNC Charlotte Department of Engineering Technology and Construction Management for their financial support. Also, thank you to Brent Summerville at Appalachian State University for his help with testing the prototype device in the Micro Hydro Test Facility. Thank you to Dr. Maciej Noras for his help with the test bench operation in Smith Hall at UNC Charlotte. And lastly, thank you to SOLIDWORKS, ANSYS, MATLAB, National Instruments and Finite Element Method Magnetics (FEMM) for use of their software.

TABLE OF CONTENTS

LIST OF TABLES

LIST OF FIGURES

CHAPTER 1: INTRODUCTION

1.1 Background

Climate change has become a major concern for individuals and governments, and the use of fossil fuels has had a hand in this phenomenon. The transition to renewable energy sources has been implemented to significantly reduce the impact the energy production industry has on the environment. It is also important to diversify energy sources because of the limited supply of fossil fuels available. This is becoming more of a concern because people are using more and more energy every year. Agencies that wish to move to renewables must overcome the inherent problem of inconsistency with renewable energy sources. When the sun does not shine, there can be no solar energy production; when the wind does not blow, there can be no wind energy production. This occurrence is forcing agencies to diversify their methods of renewable energy production to balance the inconsistencies with renewable sources and establish a reliable base load.

In hydropower production, the energy is renewable and consistent. There are many hydropower plants in existence today and as of October 2017, hydropower accounts for 7.5% of the total energy production and 44% of the renewable energy production in the United States [1]. In addition, in 2015 hydropower accounted for 24% of the global energy production [2]. However, despite being renewable, there are some negative aspects of hydropower dams that have led to an apparent cease in new large-scale dam construction. This is due to the disruption of the ecosystem, specifically, with local fish populations [3]. Most hydropower production is currently by large scale dams, however, there is significant opportunity in electrifying smaller dams.

Previously, in a time where electricity costs were very low, the construction of dams would not include power generation plants. Also, many rural small hydropower plants that existed at mills were decommissioned in the past with the expansion of the grid to rural areas. Now that electricity prices have risen significantly, and renewable sources are necessary, older dams are being updated for energy production.

The goals in the mechanical design of hydropower plants is to maximize the efficiency and reliability of the system. Increasing efficiency deals with the reduction of energy losses in different components in the design. There are several components that cause energy losses in a hydropower plant including the mechanical seal which protects the external components of the turbine and conduit from water. This component also has a limited lifetime and the reliability is uncertain. The implementation of a magnetic transmission in a hydropower plant eliminates the need for a mechanical seal and the associated losses with the component. There are several other benefits associated with magnetic transmissions that add to the reliability of the hydropower plant. The term magnetic transmission is used instead of magnetic gear because there is no effective gear ratio in the system. The purpose of the magnetic transmission is to transfer the rotational energy of the turbine inside the pipe to the outside of the pipe without the need for a sealed shaft penetrating the pipe.

The design of a seal-free micro hydropower plant has implications for increased efficiency and reliability in hydropower plants which rely heavily on the levelized cost of energy (LCOE) for determining the economic viability of the system.

1.2 Problem Statement

There is currently an opportunity for increased power generation in low flow rate, low head, rivers and streams but more robust and reliable designs are necessary to lower the levelized cost of energy (LCOE), especially in remote and off grid areas. Current designs rely on mechanical liquid seals which wear with use requiring service periodically and still require leaking water to cool the friction surfaces. With maintenance being one of the highest costs associated with hydropower turbines, the elimination of the mechanical seal will lower the LCOE making hydropower a more economically viable method of power generation. Magnetic gearing is an emerging technology that offers advantages over traditional gears. Magnetic gearing research is extensive but the implementation of the technology to real world systems is very limited. This research additionally intends to further the technical capabilities of the magnetic gear and transmission technology. Previous magnetic gear research was focused on design theory and optimization of magnetic gearing where this research will focus on the application of magnetic gearing technology in accordance to the findings in previous research on design theory and optimization.

1.3 Literature Review

For the implementation of the magnetic transmission reaction turbine (MTRT) hydropower, plant a literature review was completed to determine the current state of the art in several areas associated with this new technology. These areas can be defined as hydropower turbines, magnetic transmissions and economic viability and policy.

1.3.1 Hydropower Design

Using moving water to complete a task is a technological achievement of human kind that dates back to 4000 B.C.E [4]. Since then, many engineers in all eras have implemented similar designs to utilize the benefit of hydropower. This power can be used to complete tasks like mill grain, saw wood, hammer iron, and, most notably, generate electricity.

FIGURE 1-1: Artist painting of waterwheel used for a mill [4]

The concept of using water to power technology is not new, however, the scale of using this concept has peaked in the last century. Humans have created dams for storing water for hydropower that are so large that the earth’s rotational velocity has been impacted. The storage of river water created by the Three Gorges dam in China has increased the length of a day on earth by 0.06 microseconds according to NASA scientist [5]. The driver for creating these massive projects is power generation. Generating electricity to power modern society is a massive human effort and economical industry.

However, there is now an increased concern on the environmental impacts of the power generation industry, and it is now understood how large dams severely impact ecosystems in the environment. Modern interest in hydropower is now focused on smaller designs that have little effect on ecosystems and are economically viable. To achieve this, fish friendly and reliable hydropower plant designs are necessary. Innovation of small hydropower plants and the related components will allow for environmentally benign, distributed and economically viable micro hydropower plants to be developed.

In the hydropower industry, mechanical seals are an essential component and the added inconvenience of this component has been something the industry has had to deal with. It is not uncommon for a larger hydropower plant to pass hundreds of liters through a mechanical seal every minute [6]. This leakage is actually required to cool and lubricate the seal to prevent failure from the frictional heat generation occurring in the seal. Poor seal selection in turbine design can cause maintenance shut-downs for seal replacement multiple times a year. Maintenance on a mechanical seal often requires the turbine to go out of operation which is a significant loss in revenue. It is impractical and not cost effective to update currently existing large turbine designs to a magnetic coupling to eliminate the mechanical seal. However, in the growing industry of micro hydropower, the addition of the magnetic coupling to new turbine designs is advantageous to eliminate the need for a mechanical seal.

A review of exiting turbine geometries is necessary to understand the design considerations of turbine geometry. The turbine design is important because, if not thoroughly investigated, the energy output of the hydropower plant could be significantly less than the potential. In hydropower there are several options for turbine style which have been classified by Paish in 2002 [7]. A turbine selection graph is shown in FIGURE 1-2.

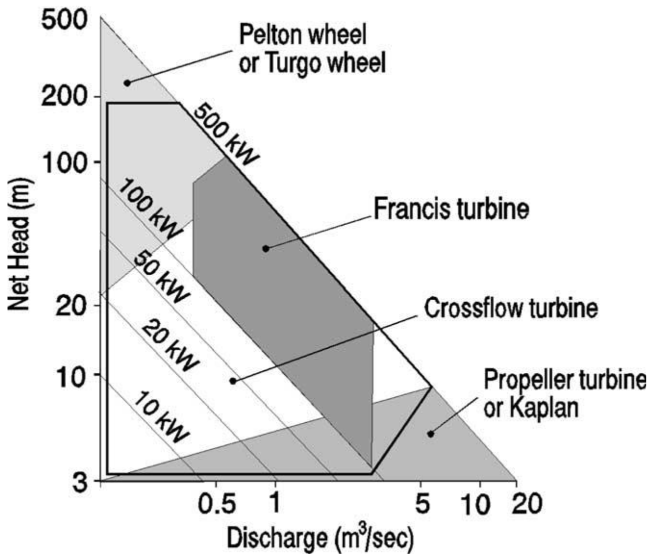

FIGURE 1-2: Turbine selection graph with net head and discharge [7]

FIGURE 1-2 is helpful for determining turbine types for larger heads and flow rates, but the low head and flow rate region is not well described, and many newer styles of turbines are not included. It is still useful because the methodologies of turbine selection are also applicable to the lower head and flow rate hydro powerplants. In 2013, Ramos et al. conducted research on a five blade reaction turbine for micro hydropower generation [8]. The research utilized CFD analysis to determine how blade geometry impacts the performance of the reaction turbine. The models were validated with testing and the power curves were established. The design Ramos et al. researched lacks an outer shroud that is required for the design used in the MTRT. In 2009, Date et al. conducted research on a reaction turbine for remote areas [9]. The research established the methods for analytically characterizing a turbine, however, the research assumed a zero seal friction loss case. In practice, the seal friction has a major impact on the energy production in a hydropower plant and should be considered. In 2011, Lucian conducted research defining the friction loss in mechanical seals with sliding rings and concluded that friction in the sealing rings develops heat which has major impact on the life of the mechanical seal [10].

A similar technology to the MTRT that exist is the Nustreem hydroelectric turbine that was designed horizontally for modular installation [11]. The 3D model of the modular Nustreem hydropower plant is shown in FIGURE 1-3.

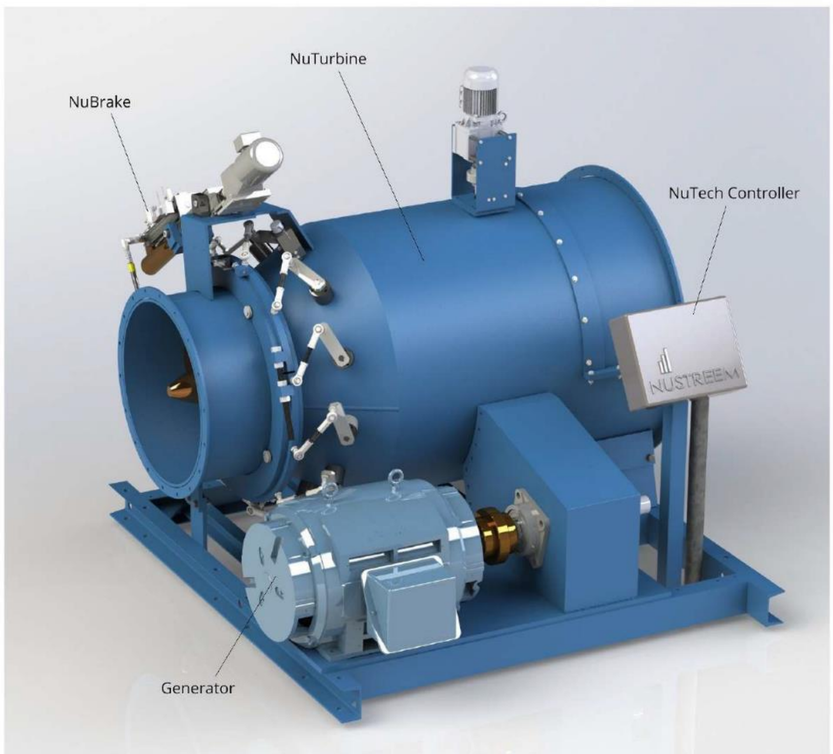

FIGURE 1-3: Nustreem modular in-conduit hydropower plant [11]

The Nustreem turbine shown in FIGURE 1-3 is modular, in-conduit and efficient but the design relies on mechanical seals around the output shaft to the generator. The use of these seals implies the continual need for service and the lowered mechanical efficiency. The use of a magnetic transmission with this type of hydropower plant design is proposed to lower maintenance requirements and improve mechanical efficiency.

Another very similar system to the MTRT is the rapidly deployable advanced integrated low head hydropower turbine developed by Fontaine et al. for generating low cost renewable energy [12]. The prototype developed by the Applied Research Lab at Penn State University is shown in the following figure, FIGURE 1-4.

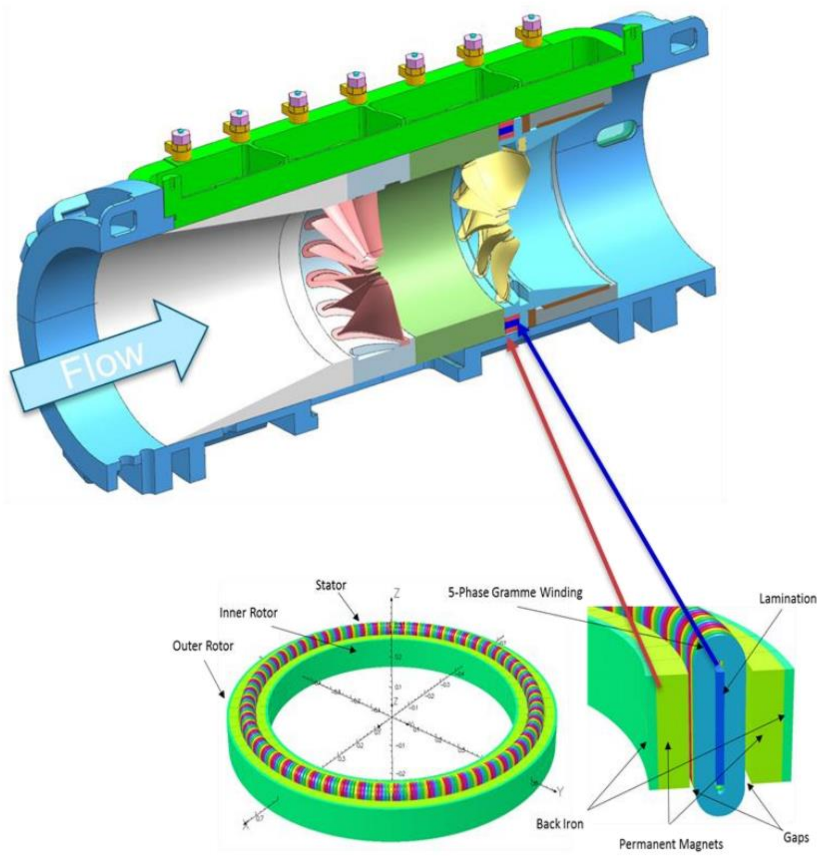

FIGURE 1-4: Rapidly deployable advanced integrated low head hydropower turbine prototype [12]

The hydropower turbine presented by Fontaine is in-conduit and modular allowing for quick implementation in currently existing hydropower sites similar to the MTRT. The use of an axial turbine that is fixed to a rotating rim is another similarity with the MTRT. The difference between the two concepts is that this system uses a direct drive generator which allows for the generation of electricity from coils in the center stator and the rotating permanent magnets on the inner rotor and outer rotor. This may increase efficiency but presents difficulties in manufacturing and power conditioning. The MTRT will transmit the power from the inner rotor to the outer rotor where it can then be handled with more standardized mechanical to electrical power take-off (i.e. belt, gearbox and generator).

One U.S. corporation has created a technology for extracting energy from utility water flow called the LucidPipe [13]. The LucidPipe is a type of hydropower plant that is capable of being placed on a water line with excess pressure head and extracting the energy to bring the pressure down to a lower value for local customers. In plumbing systems with pressure reducing valves (PRV), the LucidPipe turbine can reduce the pressure while also generating energy. This is useful for locations with high elevation reservoirs. The LucidPipe in-conduit turbine design uses a Darrius vertical axis turbine within the pipe but requires mechanical seals which incur losses. The turbine is shown in FIGURE 1-5.

FIGURE 1-5: LucidEnergy's™ LucidPipe™ [13]

This turbine also relies on mechanical seals to protect electronics and therefore there are inherent losses and a limited lifespan. The mechanical shaft used in the design also lacks features for mechanical overload protection which is inherent in a magnetic transmission. The maintenance cost associated with the LucidPipe would also be very high because repair and service would require stopping or diverting utility water flow.

The three previous in-conduit hydropower plant designs are very similar to the MTRT hydropower plant being developed in this thesis work. A comparison of the notable features of these devices is described in the following table, TABLE 1-1.

TABLE 1-1: Comparison of Similar In-Conduit Hydropower Plants

	 Nustreem [11]	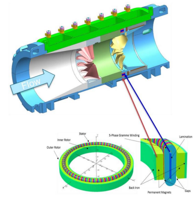 Rapidly Deployable… [12]	 LucidPipe [13]
Rated Power	75 – 250 kW	70 – 700 kW **	18 -100 kW
Commercialized	Yes	No	Yes
Includes Seal	Yes	No	Yes
Modular	Yes	No	No
High Efficiency (90% +)	Yes	Yes	No
Controlled Output Power	Yes	Yes	No
Mechanical Overload Protection	No	No	No
** - Output power specified in scalability study			

It can be observed in TABLE 1-1 that the three devices are notably different and offer different features. Subsequently, each device is designed to be used in a different hydropower application. The Nustreem is a very standard type of Kaplan hydropower plant that would most likely be used in a hydroelectric plant in a dam. The rapidly deployable advanced integrated low head hydropower turbine is ideal for low head applications, but this turbine is currently still in research and development. The LucidPipe is designed to go in utility waterflows where the speed of the water should not be impeded significantly by the turbine. The MTRT will differ from these devices based on size, design features and design complexity.

One system design also explored for micro hydropower is a pump-as-turbine (PAT) which uses standard pumps to operate as turbine and generator hydropower plants. The PAT design has been explored by Giosio et al. in 2015 and it was found that the PAT system can achieve high efficiencies in remote locations but this requires an off-design configuration and inlet flow control [14]. Further research was conducted on the PAT system by Qian et al. in 2016 on implementing a PAT system with the ability to switch between the pump and turbine configuration [15]. This is ideal in utility resource energy generation where utility services can add or remove energy to the water supply system. The style of pump in this PAT system is a tubular axial flow turbine which operates in pipe as shown in FIGURE 1-6. This design, along with the other PAT designs, also rely on mechanical seals which limit efficiency and increase maintenance cost.

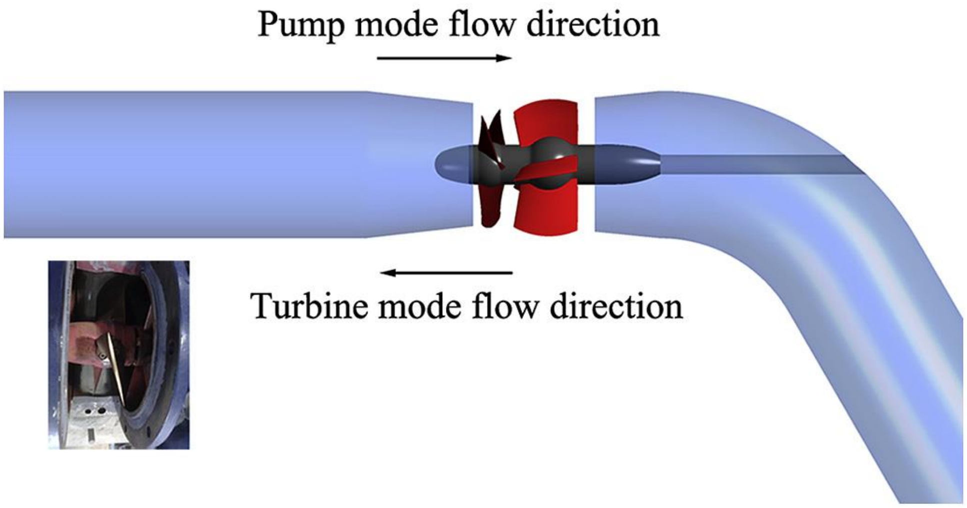

FIGURE 1-6: Diagram of tubular axial reaction turbine in PAT system [15]

Aside from standard hydropower generation from dams, this micro hydropower plant could be implemented in utility resources such as water and effluent flow. Research has been conducted into the implementation of turbines in these scenarios. In 2007, Saket et al. implemented a turbine into wastewater flow that was coupled with a system that also used photovoltaic panels to provide energy to the nearby university [16]. This research succeeded on proving the concept, however, further considerations of mechanical design are necessary for optimizing the system.

Looking further away from traditional turbine designs, there is a similar renewable energy technology called marine hydrokinetic power (MHK). Existing research from this area of turbine design is also relevant due to the turbine being axial and open centered which means the water flows through the center of the turbine. Similar styles have been implemented in MHK systems. In 2018, research has been completed for a type of turbine with water flowing through the center of the turbine with an outer shroud used for the energy conversion. The OpenHydro turbine operates similar to the

MTRT design where the water flows through the center of the turbine and turbine blades transfer the energy to a power generating rotor [17], [18]. The OpenHydro turbine design is shown in FIGURE 1-7.

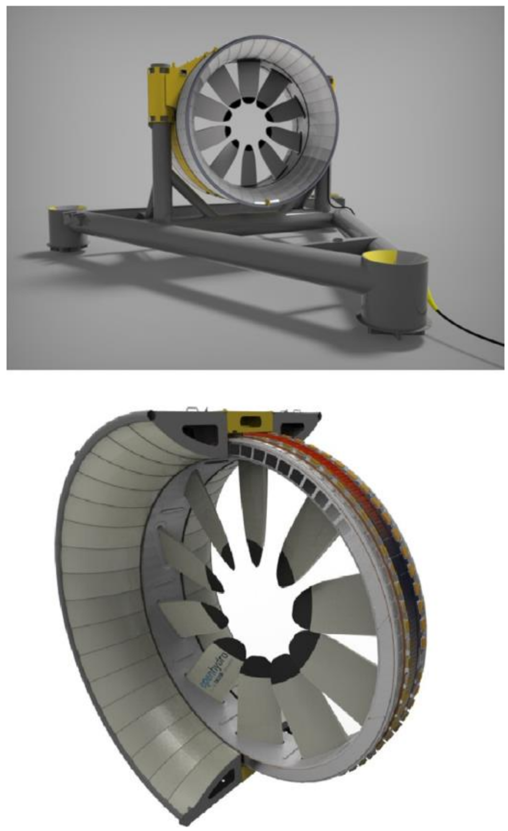

FIGURE 1-7: OpenHydro™ turbine design with outer shroud [17]

The OpenHydro turbine design has electrical windings that allow for the energy generation and this design can be adapted to include a permanent magnetic transmission for use in in-conduit flow. The current design is for tidal flow which is significantly different than hydropower flow.

1.3.2 Magnetic Transmission

The inclusion of a magnetic transmission in this new design adds a large scope of design considerations to the system. Extensive research on magnetic gears and transmissions has been conducted and this research aims to implement any relevant discoveries into a real-world application. Several magnetic gearing configurations exist but this design requires a coaxial magnetic transmission due to the axial turbine located in the pipe of the hydropower plant. Coaxial magnetic transmissions have multiple rotors that all share the same axis. The coaxial topology is shown in FIGURE 1-8.

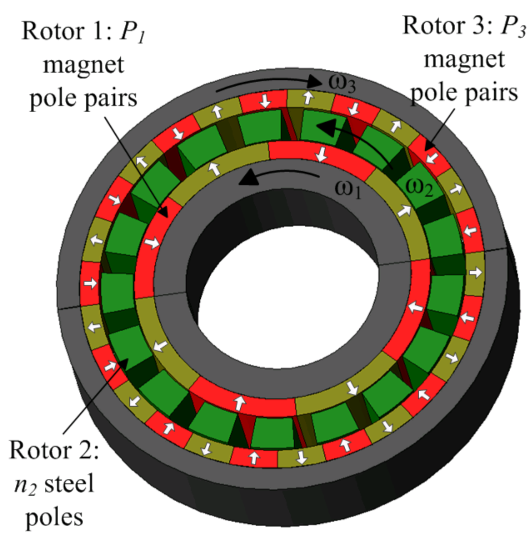

FIGURE 1-8: Coaxial magnetic gear [19]

The use of term “magnetic transmission” implies a magnetic gearbox with a unity gear ratio. Typically, magnetic gearboxes have the low speed shaft assigned to the outer or cage rotor and the high-speed shaft assigned to the inner rotor. In an in-conduit turbine hydropower plant, the rotor attached to the generator needs to be the high-speed side, therefore, the outer rotor should be the high-speed side. This creates a contradiction because the outer rotor cannot be the high-speed rotor without serious design changes in magnetic gearing topology. For the design of the MTRT, the gear ratio will be one to one and an external gear increase will be added to eliminate design challenges associated with a high-speed outer rotor in a coaxial magnetic gear.

From the invention of the first coaxial magnetic gear/transmission in 1913 there have been many advances to the technology that have allowed it to become a viable option for power transmission [20], [21]. The coaxial magnetic gear transmits power radially between the rotors using permanent magnets. For the coaxial flux focusing magnetic gear the governing equations of rotor speed and gear ratio have been presented by Atallah et al. in 2004 [22]. See FIGURE 1-9 for representation of variable in equations.

$$\omega_1 = \frac{n_2}{n_2 - p_3}\omega_2 - \frac{p_3}{n_2 - p_3}\omega_3 \tag{1.1}$$

$$n_2 = p_1 + p_3 \tag{1.2}$$

$$G_r = \frac{n_2}{p_1} \tag{1.3}$$

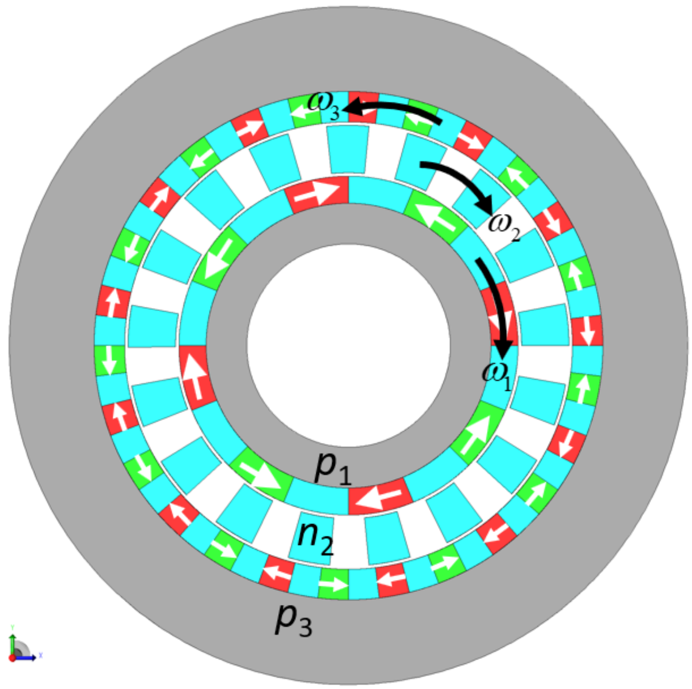

FIGURE 1-9: Coaxial magnetic gearbox with labels [23]

In these equations subscripts 1 and 3 are the inner and outer rotors, respectively and subscript 2 is the flux modulating cage rotor. Equation 1.1 describes the relationship between the rotational velocities of rotors 1, 2 and 3 ($\omega_1, \omega_2, \omega_3$ respectively) and the number of pole pairs in the rotors (p_1, n_1, p_3). Equation 1.2 describes the requirement in the magnetic topology that the cage rotor pole pairs (n_2) must be equal to the sum of the pole pairs in the inner and outer rotors (p_1, p_2). Equation 1.3 describes the gear ratio of the gearbox (G_r). Recently, there have been many advances to the coaxial magnetic gear design specifically. A comparison and timeline of recent advances in the technology is shown in TABLE 1-2.

TABLE 1-2: Literature review on coaxial magnetic gearing topologies

Topology Title	**Inventors**	**Image**	**Feature**	**Shortcoming**	**Source**
Low cost flux focusing magnetic gear [2012]	Uppalapati et al.		Rectangular ferrite magnets lower price while maintaining high capability	Ferrite magnets are subject to demagnetization and solid steel cage bars incur significant losses	[19]
Halbach [2014]	Jing et al.	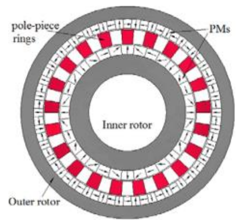	Halbach configuration minimizes torque ripple	Consideration of assembly difficulty not analyzed	[24]
Planetary with hollow cylinders [2016]	Davey et al.	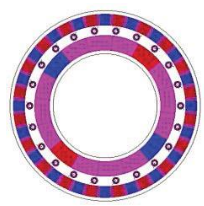	Rotating hollow cage rotor elements	Highly difficult construction and assembly	[25]
Iron segmented inner and outer rotor with PMs in cage [2016]	Fu and Li	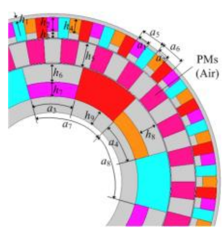	Included iron segments on inner and outer rotor maximize torque capability	Excessive permanent magnet mass greatly increases price of gearbox	[26]
Salient inner and outer rotor [2017]	Park et al.	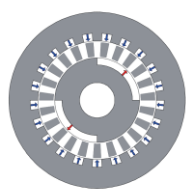	Salient topology for reduced permanent magnet mass	Consideration of assembly difficulty not analyzed	[27]
Halbach flux concentrating [2017]	Som et al.	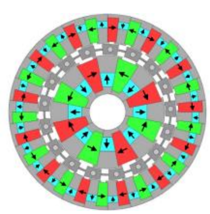	This expansion on Halbach design simplifies assembly with retaining pole	Gearbox still requires many assembly components which caused increased difficulty in assembly	[28]

From TABLE 1-2 it can be observed that the changes that are occurring with magnetic gear designs are solving problems regarding efficiency, torque transmission and torque ripple but a persistent problem is associated with the assembly of magnetic gearboxes. This research aims to apply the techniques established in the years of magnetic gearing research; however, an emphasis will be placed on the application of magnetic machine technology to the field of hydropower energy generation which requires an assembly process with minimized difficulties. Assembly is very important in magnetic gearing research and development because high magnetic forces make the manipulation of components extremely difficult.

The use of magnetic gearing to increase speed presents design challenges that may unnecessarily complicate the design of the MTRT. A solution to these design challenges is to use a magnetic coupling instead of a magnetic gear in the transmission. The coupling lacks a cage rotor and the inner and outer rotors are co-rotational. The coupling still allows for isolation between the inside and outside of the conduit and the elimination of the mechanical seal in the design. Magnetic couplings have been implemented in many technologies and the mechanics are understood. Research by Charpentier and Lemarquand described the calculation of magnetic forces in ironless permanent magnet couplings [29]. The following figure shows a diagram of the magnetic coupling and the ideal configuration of the permanent magnet polarities; see FIGURE 1-10.

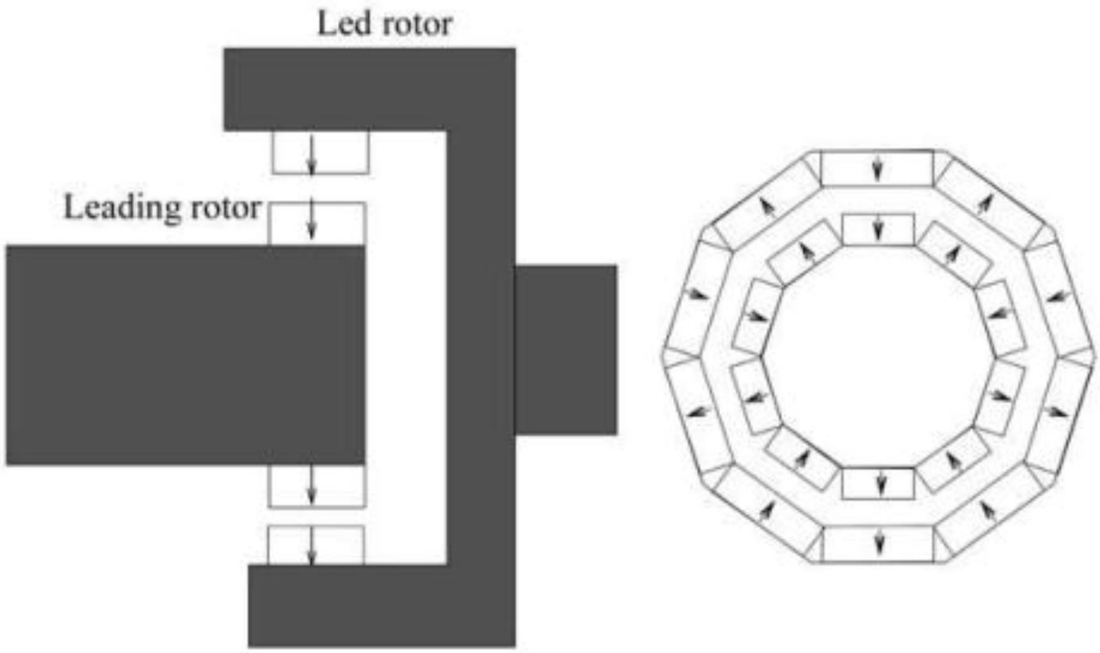

FIGURE 1-10: Cylindrical air gap magnetic coupling [29]

It can be observed in FIGURE 1-10 that the alternating polarity is optimal for the configuration of the permanent magnets in the coupling. The research presented by Charpentier and Lemarquand determined the torque transmission of the coupling is calculated with the following equation.

$$T = 2p\left(\sum_{i\ \in\ \text{rotor 1}} F_t\left(i\right).r_2\right)\ [29] \tag{1.4}$$

In this equation, the torque, T , is determined by the number of pole pairs, p , the tangential component of magnetic force, F_t , and the radius of the second rotor in the coupling, r_2 . The tangential magnetic force can be determined from solving Maxwell’s equations which warrants the use of computer simulation.

1.3.3 Economics

In the course of this research, a hydropower plant will be designed, however, the ultimate success also relies on the creation of an economically viable alternative to current hydropower plant design. This requires an analysis on the energy production capabilities of this hydropower plant and a comparison to other forms of hydropower. In 2015, Elbatran et al. completed a comparison of the current method of micro hydropower generation [30]. From this research, a very well described cost analysis for the different types of micro hydropower methods is presented. Another analysis was completed by Zema et al. in 2005 which established a method to evaluate the economic viability of micro hydropower plants in irrigation systems [31]. The focus of this research was specifically on agriculture, but the findings can be translated to other industries. This method also identifies some indications for micro hydropower installations that must be considered before installation. One case study, completed by Thorburn and Leijon in 2005, discusses a real hydropower system that was implemented in Sweden [32]. The research discusses the power generation implications for grid connection which is another driver of the economic viability of a hydropower plant.

In considering the impact of applying this new technology an analysis of the opportunity that exist must be completed based on location and the water flow characteristics. A thorough study of the potential of hydropower in the United States was completed by Kosnik in 2008 [33]. It is apparent that in every state there is opportunity for hydropower energy generation. Another very important aspect of this research is the inclusion of the upgrade potential of currently existing dams in the United States. This data is shown in

FIGURE 1-11.

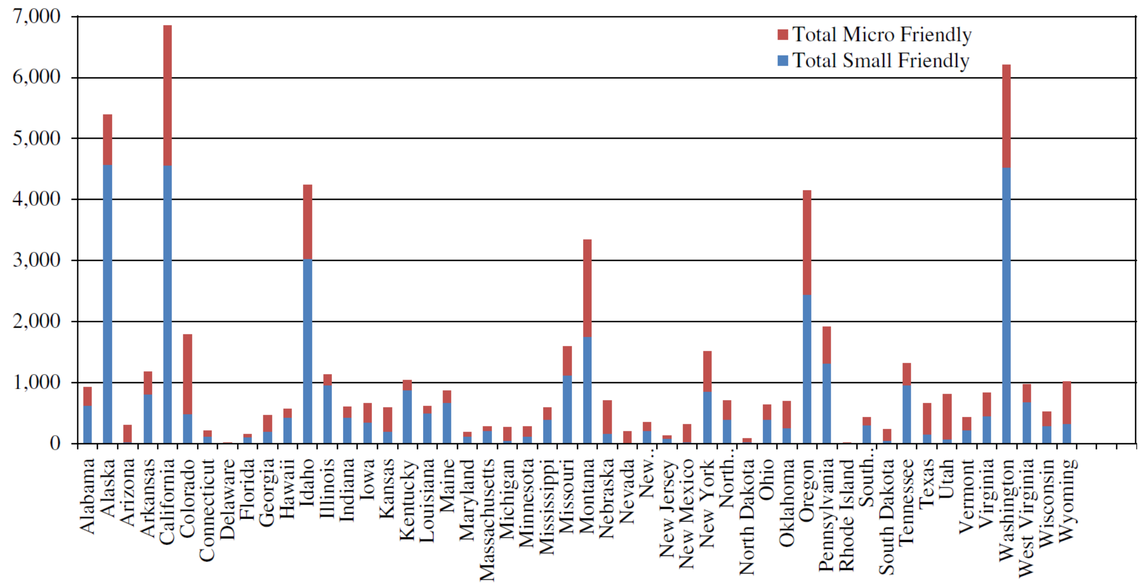

FIGURE 1-11: U.S. small and micro hydropower potential by state (MW) [33]

From this research, it can be concluded that the opportunity for 60 GW of hydropower is real and it can be alluded to that further advancement in the design of micro hydropower plants is necessary to take advantage of the current potential. The economic viability of installing hydropower is heavily reliant on the civil cost of the installation and the maintenance and repair necessary in the life of the powerplant. Advancing hydropower into more modular systems that require less civil work and are more robust is essential to harnessing this potential.

The policy regarding the implementation of micro hydropower plants is another driver of the economic viability. In a very detailed report created by Kelly-Richards et al., the energy policy for micro hydropower plants is discussed and with a major focus on the environmental protection aspects of implementing the technology [34]. The protection of the environment is extremely important, and it is important to understand the policy to ensure projects adhere to government code.

1.3.4 Conclusion

In conclusion, it is apparent that opportunity for power generation exists and the advancement of the industry with novel and innovative plant designs is necessary. This is not only an economically safe investment but also an investment in the protection of the environment with the transition to renewable energy sources. The implementation of concepts from reaction turbine and magnetic transmission research allows for a design of a micro hydropower plant that will move towards increased efficiency and reliability in micro hydropower affectively lowering the LCOE which is the most important deciding factor in micro hydropower plant investment.

1.4 Research Significance

Due to the rising cost of energy, the increased demand of energy and the movement to renewables to reduce environmental stress, this research is being completed to advance the energy field by providing a low-cost, modular, renewable energy technology. The introduction of the MTRT continues the move toward new micro hydropower plants with more robust designs, lower installation cost, lower maintenance requirements and subsequently, a lower cost of energy. This research will develop a prototype MTRT hydropower plant at a small scale and describe the analysis and testing of the prototype device.

CHAPTER 2: METHODOLOGY

2.1 Design Method

The design methodology has been structured in order to optimize the system to achieve an efficient and robust design that is capable of being installed by a two-person team. Attention to the individual sub-systems is required to achieve a successful and integrated design. To organize the sub-systems in need of consideration in the design, an energy flowchart is used as shown in FIGURE 2-1.

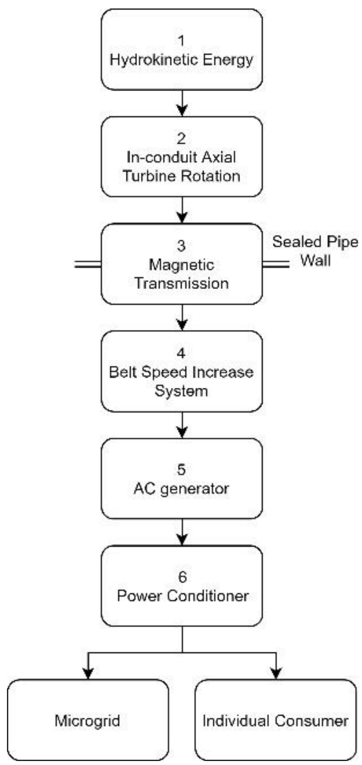

FIGURE 2-1: System energy flowchart

The energy flowchart describes how the energy that originates from the hydrokinetic energy of moving water, is converted into useful electrical energy for grid and non-grid use. The energy contained by moving water is quantifiable through analytic equations but the conversion of hydrokinetic energy into rotational mechanical energy in a turbine requires advanced computational fluid dynamic (CFD) analyses. These analyses are necessary to optimize turbine geometry and achieve high efficiency. The parameter that defines the efficiency is the coefficient of performance, C_p. The CFD analyses can also determine the pressure loading of the turbine in use, which in turn can be used for the mechanical analysis of the turbine. The energy flows from the turbine to the magnetic transmission where it is then transmitted through the pipe walls with magnetic forces. A magnetic analysis is required to reduce the losses in the magnetic transmissions and to determine the load carrying capacity of the magnetic transmission before pole slipping. This factor of load carrying capacity is a major component of system robustness because if the magnetic transmission cannot carry significant load, significant power cannot be produced. With the data generated from the CFD and magnetic analysis, a mechanical analysis can be completed that will determine the mechanical robustness of the load carrying components in the system and prevent failure in standard operating conditions. To account for extraordinary operating conditions, factors of safety will be implemented within the constraints of material cost, component weight, manufacturability and overall size.

The following sections in this chapter will describe the methods used to complete the analyses of the system. There are equations that are analytically solvable, however, a significant portion of the equations require the use of computer software to solve and generate useful data. The analyses rely heavily on the use of finite element (FE) simulation.

2.2 Computational Fluid Dynamics Method

Computational Fluid Dynamics (CFD) is a valuable tool for simulating the dynamics of fluid motion. In the design of hydropower turbines, it serves the purpose to characterizing the flow of water through the turbine. The power of flowing water can be determined from the analytic equation shown below.

$$P_{hk} = \frac{1}{2}\rho A v^3 \tag{2.1}$$

In this equation, the hydrokinetic power, P_{hk}, is dependent on the water density, ρ, the pipe cross-sectional area, A, and the water flow velocity though the pipe, v. Because of the cubic, the velocity of the water is the most significant parameter in the power of flowing water. The bridge between the power of flowing water and turbine power is the coefficient of performance, C_p. The equation of turbine power, P_t, can be describe using the following equation.

$$P_t = C_p \cdot \frac{1}{2}\rho A v^3 \tag{2.2}$$

The coefficient of performance is the parameter to optimize in the design of a turbine. The coefficient is not typically determined analytically and instead requires the use of CFD simulation. This form of FE simulation is fundamentally based on the Navier-Stokes (N-S) equations which can be used to determine the more detailed characteristics of flow such as pressure and velocity at specific locations within the domain. The first equation of the N-S equations is the continuity equation which is shown below.

$$\frac{\partial \rho}{\partial t} + \nabla \cdot (\rho \vec{U}) = 0 \tag{2.3}$$

The continuity equation describes the conservation of mass in a system. The net mass flow in a system is zero because mass cannot be created or destroyed. This form of the equation accounts for the compressibility of fluids or the change of density over time. This is an important factor in a lot of fluid flows, however, it is safe to assume that water is incompressible in an axial flow turbine. With an incompressible fluid the continuity equation simplifies to the following equation.

$$\nabla \cdot \vec{U} = 0 \tag{2.4}$$

In this equation, the vector $\vec{U}$ is equal to $(u,\ v,\ w)$, therefore the divergence of $\vec{U}$ is zero meaning no mass is created or destroyed. The next component of the N-S equations if the momentum equation. In Cartesian coordinates, the momentum equation is as follows.

$$\frac{\partial \vec{U}}{\partial t} + \nabla \cdot \left(\vec{U}\vec{U}\right) = -\nabla p + \nabla \cdot \left(\nu \nabla \vec{U}\right) \tag{2.5}$$

This equation describes the interaction of fluid in movement by equating the inertia of fluid mass and the divergence of stress within a volume of flow with specific boundary conditions. This equation is fundamental to fluid flow but to generate useful data in FE software with limited computational capabilities a few assumptions can be made to simplify the calculation. The flow through a turbine is turbulent which complicates the simulation but Reynolds-averaged Navier-Stokes (RANS) equations can be used to allow for the simulation of these turbulent and transitional flows. The Reynolds stress equations is very commonly used in turbulent flow simulations. This equation, presented by William K. George, is shown below [35].

$$
\begin{aligned}
&\frac{\partial}{\partial t}\langle u_i u_k\rangle + U_j\frac{\partial}{\partial x_j}\langle u_i u_k\rangle = \left\langle \frac{p}{\rho}\left[\frac{\partial u_i}{\partial x_i}+\frac{\partial u_k}{\partial x_k}\right]\right\rangle \\
&+\frac{\partial}{\partial x_j}\left\{-\frac{1}{\rho}\left[\langle p u_k\rangle\delta_{ij}+\langle p u_i\rangle\delta_{kj}\right]-\langle u_i u_k u_j\rangle+2\nu\left[\langle s_{ij}u_k\rangle+\langle s_{kj}u_i\rangle\right]\right\} \\
&-\left[\langle u_i u_j\rangle\frac{\partial U_k}{\partial x_j}+\langle u_k u_j\rangle\frac{\partial U_i}{\partial x_j}\right] \\
&-2\nu\left[\left\langle s_{ij}\frac{\partial u_k}{\partial x_j}\right\rangle+\left\langle s_{ij}\frac{\partial u_i}{\partial x_j}\right\rangle\right]
\end{aligned}
\tag{2.6}
$$

This equation commonly used is notably different than the N-S equations because the 5 terms to the right of the equal sign represent the pressure-strain rate term, the turbulence (or divergence) term, the production term and the dissipation term respectively [35].

Modeling the turbulence in a turbine is essential to obtaining accurate results. The effect of turbulence on the turbines efficiency and loading is significant, therefore a CFD solver must also solve the turbulence in the flow. There are several models for computing the turbulence in flows but in axial flow hydro turbines, the k- ω shear stress transport (SST) model is the most common model for obtaining accurate results with lower calculation times compared to other turbulence models. This is due to the model's reliability in adverse pressure gradients and separating flow, as well as the low sensitivity to inlet free-stream turbulence properties. The model for turbulence kinetic energy is shown below [36].

$$
\frac{\partial k}{\partial t}+U_j\frac{\partial k}{\partial x_j}=P_k-\beta^* k\omega+\frac{\partial}{\partial x_j}\left[\left(\nu+\sigma_k\nu_T\right)\frac{\partial k}{\partial x_j}\right] \text{ [36]} \tag{2.7}
$$

This equation describes the generation of turbulent kinetic energy in flow and the following equation describes the specific dissipation rate.

$$\frac{\partial \omega}{\partial t}+U_j\frac{\partial \omega}{\partial x_j}=\alpha S^2-\beta\omega^2+\frac{\partial}{\partial x_j}\left[\left(\nu+\sigma_\omega \nu_T\right)\frac{\partial \omega}{\partial x_j}\right]+2(1-F_1)\sigma_{\omega 2}\frac{1}{\omega}\frac{\partial k}{\partial x_i}\frac{\partial \omega}{\partial x_i} \tag{2.8}$$

The calculation of the k-ω SST equations is part of the CFD solving which is to be completed in ANSYS Fluent. The inclusion of this model will allow for more accurate results to be generated by the CFD solver.

The computation of the equations used in the CFD solver is dependent on boundary conditions defined in the model. The most important boundary conditions are the inlet, outlet and walls. The inlet defines the characteristics of the fluid entering the domain. This can be defined several ways but most commonly an as inlet velocity. Similarly, the outlet can be defined in several ways but often by an outlet pressure. In both the inlet and outlet boundary conditions the quantity of turbulence must be defined. CFD simulation also relies on the zero-slip condition at walls. This means the velocity of the fluid touching a wall is always zero and this creates the shear stresses seen in fluid flow. The wall boundary condition is very important in turbine modeling because turbine blades are technically walls and the effect of the fluid on these walls defines the drag and lift forces on the blade that cause rotation and energy conversion.

2.3 Magnetostatic Analysis Method

The magnetostatic analysis is to be completed with the use of a finite element magnetic solver. The software chosen for the analysis is an open-source solver titled FEMM (Finite Element Method Magnetics) [37]. This software solves Maxwell’s equations in 2D planar or axisymmetric through the use of finite elements. This software is effective for low frequency simulations that use permanent magnets.

To understand the mechanics of the software, Maxwell's equations must be understood. The first component of Maxwell's equations is Coulombs law which defines that the divergence of an electric field, E, equals the electrical charge density, ρ, over the permittivity of free space, ε_o.

$$\nabla \cdot E = \frac{\rho}{\varepsilon_o} \tag{2.9}$$

The second component defines that the divergence of the magnetic flux density, B, equals zero.

$$\nabla \cdot B = 0 \tag{2.10}$$

The third component, known as Faraday's Law, defines that the curl of the electric field equals the negative time rate of change of the magnetic flux density.

$$\nabla \times E = \frac{-\partial B}{\partial t} \tag{2.11}$$

The fourth component is Ampere's Law with Maxwell's addition and it defines that the curl of the magnetic flux density equals the permeability, μ_o, multiplied by the electric current, J, summed with the permeability multiplied with the permissively and the time rate of change of the electric field.

$$\nabla \times B = \mu_o J + \mu_o \varepsilon_o \frac{\partial E}{\partial t} \tag{2.12}$$

These equations are used to define electromagnetics and can be applied in real applications to simulate fields and fluxes in magnetic machines. The term, H, for magnetic field intensity can also be used to describe the physics of a magnetic field and it relates to the flux density by multiplication of the permeability.

$$B = \mu_o H \tag{2.13}$$

The curl of this magnetic field defines the electric current.

$$\nabla \times H = J \tag{2.14}$$

FEMM uses these equations to simulate the physics of magnetism and it does this by solving for a field that satisfies Maxwell's equations with a magnetic vector potential approach [38]. The approach solves the flux density in terms of the vector potential, A.

$$B = \nabla \times A \tag{2.15}$$

With this approach the relationship between current and magnetic flux density can be rewritten with this magnetic vector potential.

$$\nabla \times \left(\frac{1}{\mu(B)} \nabla \times A \right) = J \tag{2.16}$$

This equation is valid for a case of nonlinear permeability in a material and it can be simplified further when the material permeability is linear and the material is isotropic.

$$-\frac{1}{\mu_o} \nabla^2 A = J \tag{2.17}$$

The overall purpose of the magnetostatic analysis is to understand the magnetic forces present in the magnetic transmission of the powerplant. Maxwell's equations defined above are solved in the simulation and then with post-processing, useful information can be extracted from the simulation results. The information that is desired from the simulation of the magnetic transmission is the peak torque that can be achieved by the magnetic transmission. This requires solving for the resultant magnetic forces that the permanent magnets are exerting between the inner and outer rotor. Fortunately, FEMM has a postprocessing function to calculate the torque present due to magnetic forces. The torque is calculated using a steady-state weighted stress tensor. This allows for the calculation of a non-uniform distributed force per unit area at the interface between two separate materials [39]. In this case, the force per unit area will be calculated between the permanent magnets and the surrounding air gap. The Maxwell stress tensor, σ_{ij}, can be calculated using the vector components in the magnetic flux density.

$$\sigma_{ij} = \frac{1}{\mu_o}\left(B_i B_j - \frac{1}{2}\delta_{ij} B_k B_k\right) [39] \tag{2.18}$$

From the stress tensor the traction between two materials (a and b) can be solved with cylindrical coordinates which are necessary for circular rotor geometries. These are divided into traction in the normal (r) and tangential (θ) directions.

$$f_r \approx \sigma_{rr}^a = \frac{1}{2\mu_a}\left(B_r^2 - B_\theta^2 - B_z^2\right) \tag{2.18}$$

$$f_\theta \approx \sigma_{r\theta}^a = \frac{1}{\mu_a}\left(B_r B_\theta\right) \tag{2.19}$$

The final step with post-processing is to compute the resultant torque, T, from the tangential traction through the use of the surface integral with reference to the actual geometry of the machine.

$$T = \oint r \times f_\theta d\Omega \tag{2.20}$$

FEMM completes this post-processing calculation automatically with a function called *mo_blockintegral* which requires the input of the desired block. The various areas within the model that represent different materials such as magnets, steel, or air are assigned to a block. The block integral of weighted stress tensor is calculated for one set of rotor magnets to find the torque between the two rotors of the magnetic transmission. This process can be applied to find the peak torque in the magnetic transmission through a process of rotating the magnetic components in one rotor of the model a finite angular displacement about the central axis and recalculating the torque between the rotors. As one rotor of magnets rotates, the torque between the rotors should increase and then decrease as the magnets move out and back into phase. This essentially forms a magnetic spring coupling that after rotated past the peak torque and associated angular displacement cogs into the next point of equilibrium in the magnetic transmission.

The analysis of the magnetic transmission used in this thesis research is presented in section 4.2. The magnetic transmission will be analyzed using FEMM to determine peak torque and to compare different magnetic and nonmagnetic materials for the yoke of the rotors in the transmissions. This multistep analysis is completed with MATLAB to automate the simulation with an independent variable of rotor rotational displacement in degrees and a dependent variable of torque between rotors of the magnetic transmission in newton meters (Nm); see section 4.2.

2.4 Mechanical Analysis Method

The mechanical analysis involves the selection of purchased load carrying components (i.e. bearings and belts) and the analysis of stress in load carrying components through the use of FEA software. The mechanical analysis of stress will be completed with the ANSYS Mechanical software and the results will be analyzed using the von Mises yield criterion. ANSYS Mechanical is a very widely used software in mechanical analysis capable of producing reliable results.

The use of von Mises yield criterion allows for the determination of material failure in 3-dimensional stress with yield strength parameters determined from uniaxial stress testing. The von Mises stress is used commonly in the analysis of ductile materials such as metals and plastic, therefore it is applicable in the plastic prototype components in the design of the MTRT. The von Mises yield criterion is shown below [40].

$$\frac{1}{6}[(\tau_{11}-\tau_{22})^2+(\tau_{22}-\tau_{33})^2+(\tau_{33}-\tau_{11})^2+6(\tau^2{}_{12}+\tau^2{}_{23}+\tau^2{}_{13})]=k^2 \tag{2.21}$$

The material is predicted to yield when the components of stress tensor, τ, are greater than the criterion. The pure shear yield stress, k, is commonly determined through experiments in uniaxial testing and can be established with the simple tension elastic limit, S_y, as shown in the following equation.

$$\frac{S_y{}^2}{3}=k^2 \tag{2.22}$$

The von Mises equivalent stress, S_v, determined by the Cauchy stress tensor is shown in the following equation.

$$\sqrt{\frac{(\tau_{11}-\tau_{22})^2+(\tau_{22}-\tau_{33})^2+(\tau_{33}-\tau_{11})^2+6(\tau^2{}_{12}+\tau^2{}_{23}+\tau^2{}_{13})}{2}}=S_v \tag{2.23}$$

The criterion dictates that yielding will occur when the von Mises equivalent stress exceeds the simple yield limit stress of the material. This is shown in the following equation.

$$S_v \geq S_y \tag{2.24}$$

This is a theoretical approach to determine failure in mechanical components, however, there are some uncertainties associated with the determination of this stress in practice. Namely, this criterion relies on the relation of yield tensile strength to be $\sqrt{3}$ times greater than the yield shear strength which is not always the case. To compensate for the uncertainties, a factor of safety will be instituted to prevent component failure. The measure of the robustness of the components will be the factor of safety which is a ratio of the maximum stress to the yield strength of the material yield strength. The factor of safety calculation is shown in the following equation.

$$FoS = \frac{S_y}{S_v} \tag{2.25}$$

The factor of safety should be significantly greater than 1 but also not too high (~50 +) and the purpose of the range is to ensure that the components will not fail while also not over designing components which unnecessarily increases cost. Limiting the factor of safety is only needed in components with high costs of manufacturing.

CHAPTER 3: MECHANICAL DESIGN

The mechanical design of the powerplant is a major portion of the work in developing the new technology. This section will describe the details of how the system is designed to allow for the desired function of energy conversion. There are some extraordinary design conditions that warrant design strategies that are not typically used in mechanical design.

First, to better understand how the design will be implemented in the system, a model of the powerplant in use in a small dam has been generated. This is shown in the figure below.

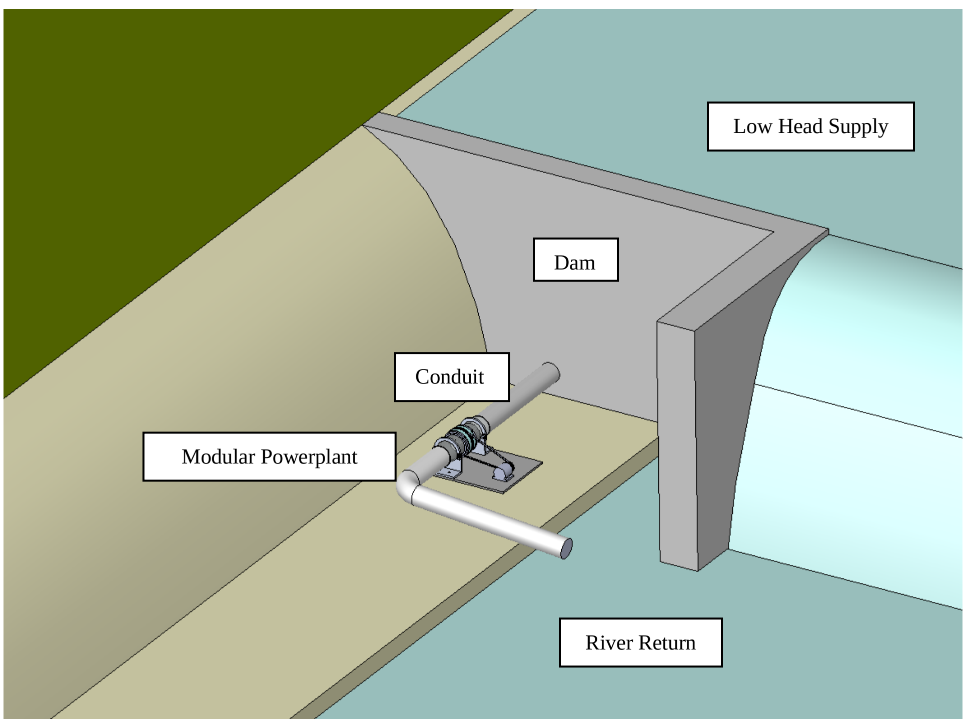

FIGURE 3-1: Powerplant in small dam construction

As shown in the figure above, the powerplant is located in a runner pipe connected to the higher head side of the dam. This creates an energy potential and causes the pressure difference which causes the water to flow. The energy in this flowing water can be captured by an axial turbine. The design of the axial turbine is shown below.

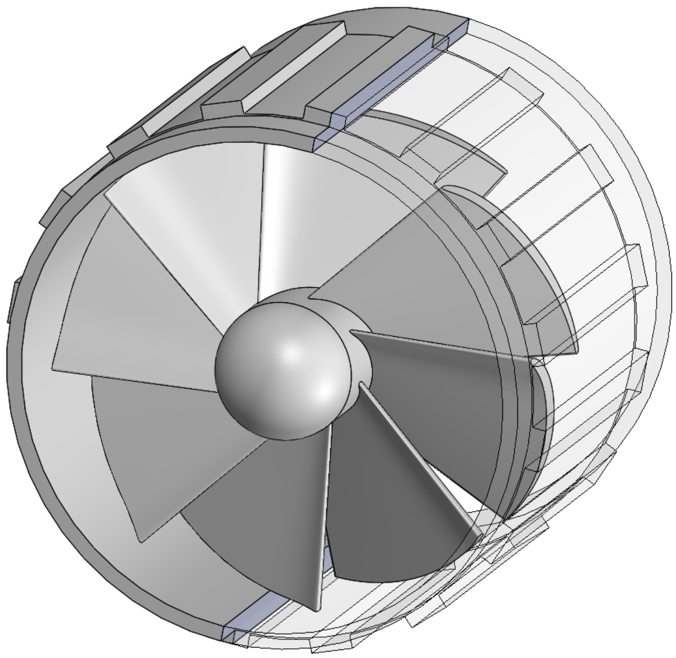

FIGURE 3-2: Modular axial turbine in MTRT

The axial turbine shown above has 8 blades that are set at a 60 degree pitch and have the profile of a NACA 64006 airfoil. This airfoil profile is characterized by its lift coefficient of 0.9, its camber position of 20% standard and its thickness of 6%. The airfoil itself is shown in the figure below.

FIGURE 3-3: NACA 64006 airfoil profile

This airfoil was selected to achieve a high lift coefficient, which will increase the obtainable torque from the water flowing past it. This was an initial airfoil selection and configuration and can be updated with improved CFD characterization based on site-specific flow parameters. This is realized in the field through the use of a modular turbine rotor geometry enabled by advanced manufacturing techniques. As the geometry of the airfoil and turbine change, the rotor remains constant which allows for reconfiguring the system assembly. The full system assembly which houses the turbine is shown below in FIGURE 3-4.

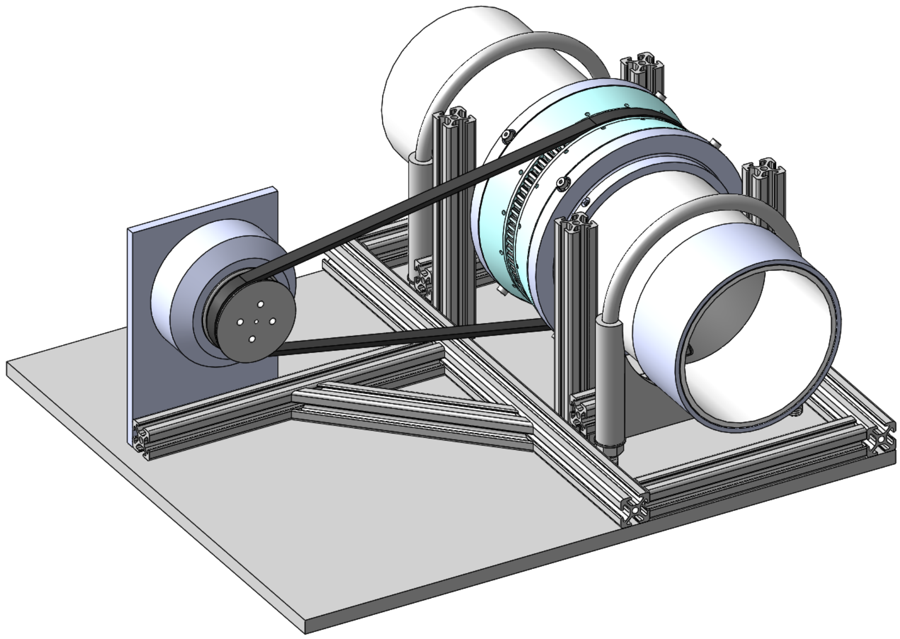

FIGURE 3-4: 3D model of system assembly

From the model, it can be observed that the powerplant is in-conduit allowing it to be easily implemented in currently existing pipes. To lower cost, a design goal was to keep geometries as simple as possible to lower manufacturing prices and to decrease assembly time. A section view into the powerplant allows for a more revealing view of the inner workings of the system. This is shown below in FIGURE 3-5.

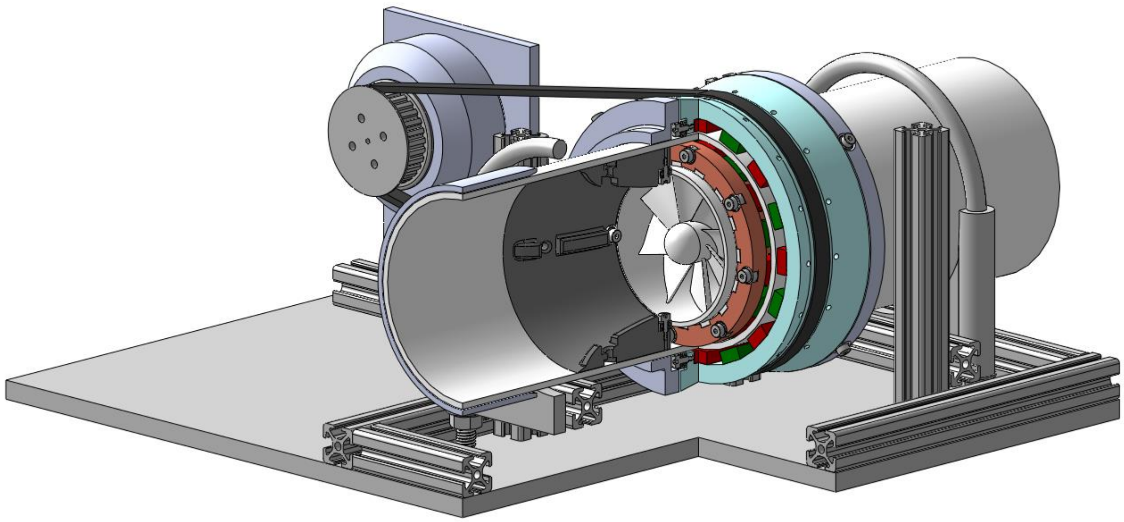

FIGURE 3-5: Section view of powerplant

The section view reveals the inner components of the powerplant. The pipe is shown in translucent gray, the guide vane is shown in dark gray, the permanent magnets are shown in red and green, the turbine is shown in white, the inner rotor is shown in orange and the outer rotor is shown in light blue. The inner and outer rotor are both fixed axially but free to rotate. The magnetic transmission fixes these rotors co-rotationally. This allows for the non-contact power transmission through the pipe wall. The rotation of these rotors requires the use of bearings to limit the friction losses associated with rotation. The bearings used in the design are categorized into axial positioning bearings and radial positioning bearings. As the title suggest, the axial positioning bearings fix the rotors axially and compensate for any axial thrust load applied by the flowing water. The radial positioning bearings allow the rotors to rotate freely either in the pipe (inner rotor) or out of the pipe (outer rotor). The bearings can be seen in the figure below.

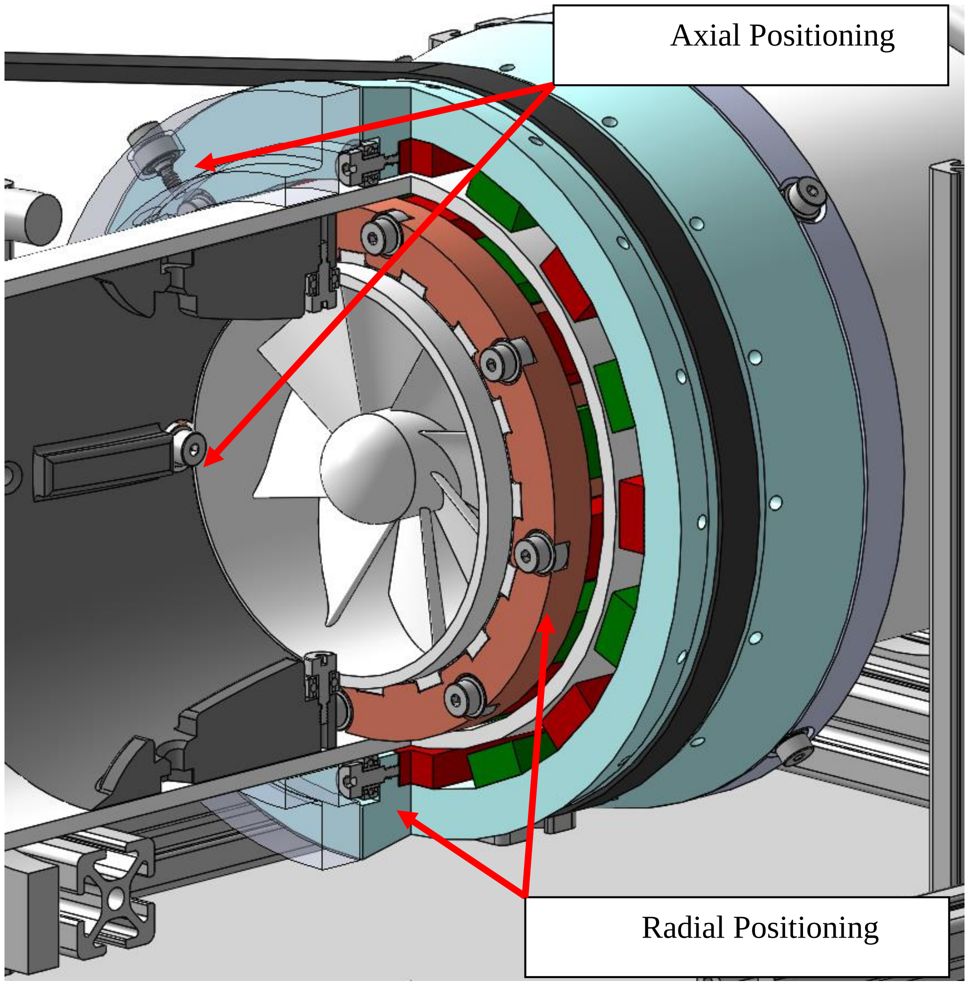

FIGURE 3-6: Bearing configuration

From the figure the axial positioning and radial positioning bearings can be observed. The bearings are designed to be low cost and easily implemented in the prototype, but there is uncertainty about the performance and therefore, scaling up will require redesign of the bearing configuration.

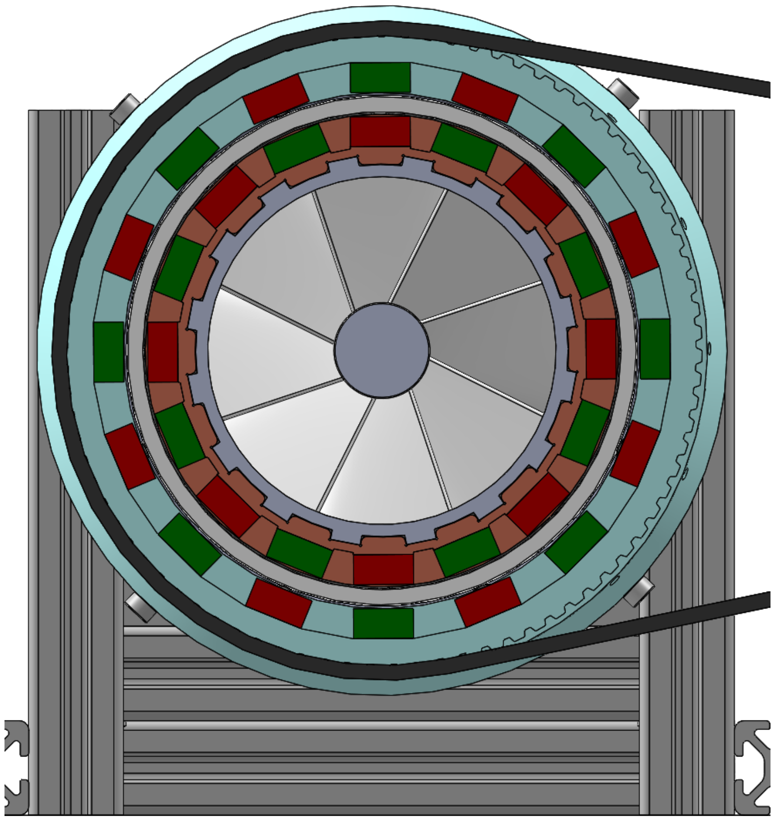

FIGURE 3-7: Cross section-view of turbine and magnetic transmission

From this figure the magnetic transmission is revealed. The red and green magnets represent the direction of the polarity of the magnetization of the permanent magnet. In other words, the green magnets have polarity that points radially towards the center axis and the red magnets have polarity that point radially outwards. In a permeant magnet the polarity direction determines which face is north and which face is south. The magnets selected in this design have the larger face polarized as shown in the figure below.

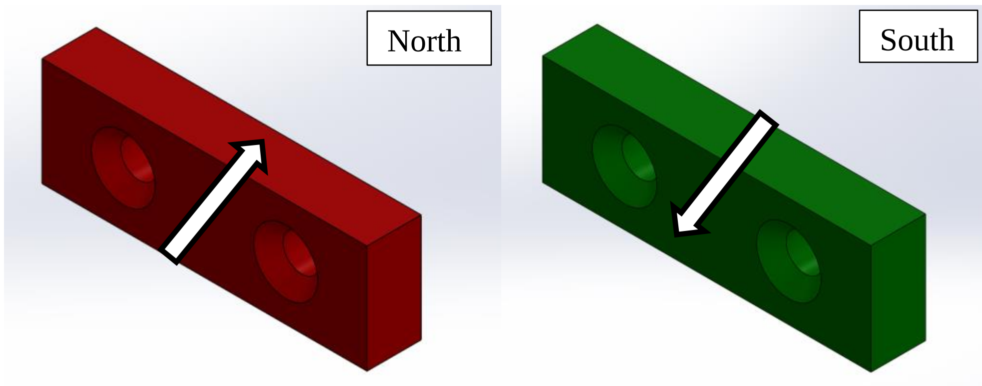

FIGURE 3-8: Permanent magnet polarization

In FIGURE 3-8 the two magnets are the same, the color is used to represent the direction of the polarization. The layout of the alternating magnet polarity in the magnetic transmission can be seen in the following figure, FIGURE 3-9.

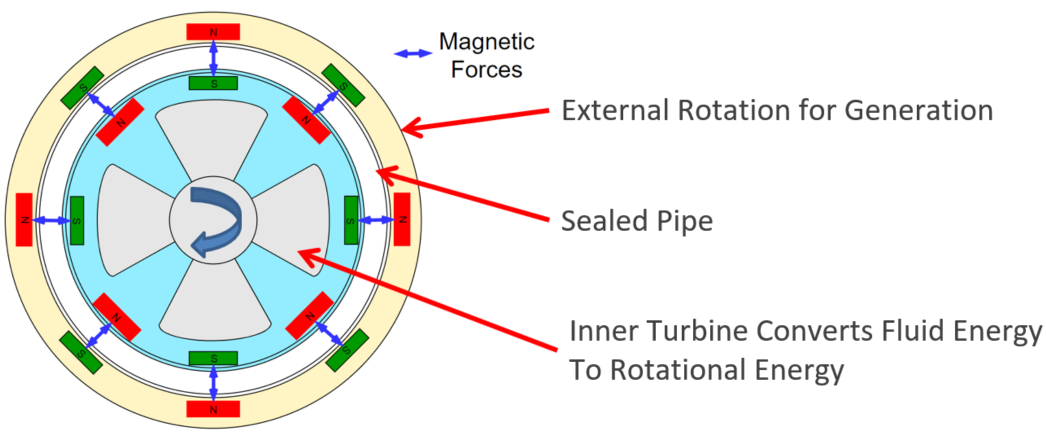

FIGURE 3-9: Magnetic transmission schematic

It can be observed in FIGURE 3-9 that the polarity of the magnets alternate around the circumference of the magnetic transmission. This layout was found to be the ideal configuration of a magnetic transmission in the literature review on magnetic couplings [29].

In conclusion, the mechanical design is kept as simple as possible to lower cost and simplify assembly. The mechanical design for this prototype is specific to a small 4 inch pipe and scaling up would require redesign of some elements. At this small scale the effectiveness of the turbine can be characterized with design analysis.

CHAPTER 4: DESIGN ANALYSIS

4.1 Computational Fluid Dynamics Analysis

4.1.1 Problem Definition

The purpose of completing an analysis with computation fluid dynamics (CFD) is to predict the interaction between the water flowing through the hydropower plant and the turbine extracting the energy. The fluid pressure load (FPL) is important to understand to ensure the design is structurally robust. CFD is also useful to characterize the performance of the turbine and it allows for iterative design changes to improve efficiency. The use of CFD in this research will only seek to ensure the robustness of the turbine design in the water flow.

The model used to simulate the FPL is a 3D volume of fluid model in which the solid part represents the fluid in the conduit and around the turbine. The model is made by subtracting the volume of the turbine from the volume of the water in the conduit to cause a void in the fluid where the turbine would be. This generates walls where the turbine blade walls would be. The volume of fluid with the inserted turbine can be seen in the following figure, FIGURE 4-1.

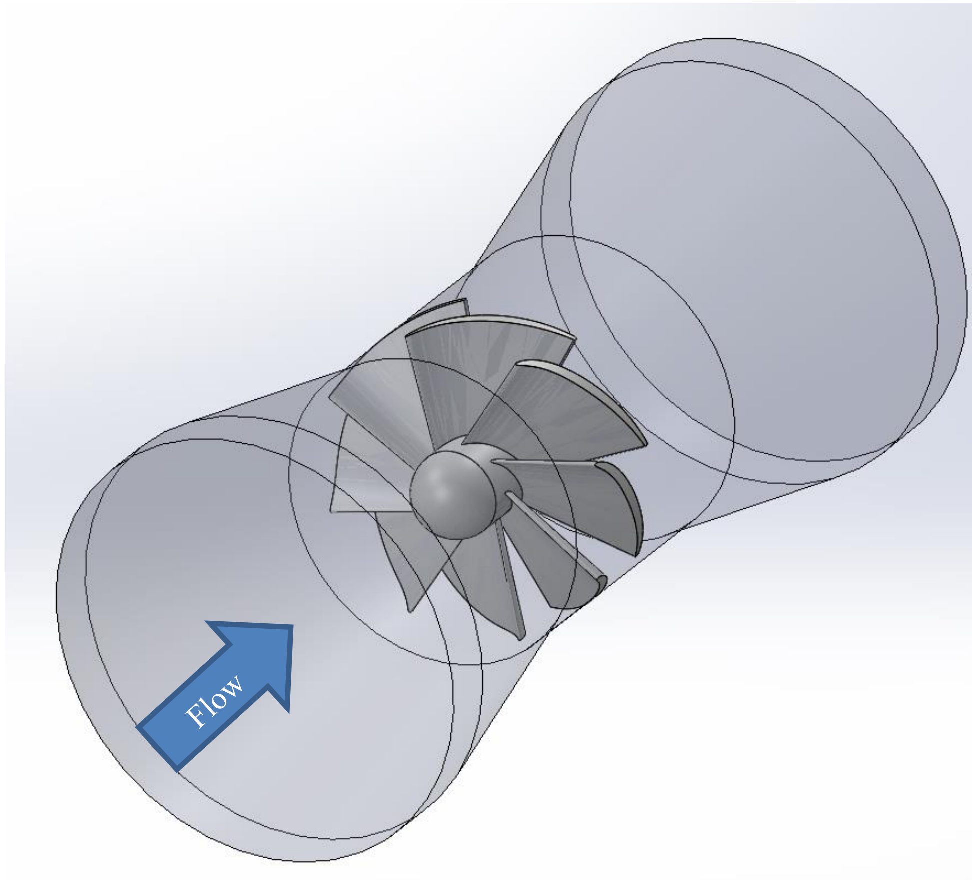

FIGURE 4-1: Volume of fluid model in SOLIDWORKS

The turbine blades and central hub can be seen in FIGURE 4-1. The axial length of the volume of fluid is 8.8 inches, and the length is limited by the computational cost associated with larger meshes. In this application of FPL simulation, a longer inlet and outlet volume is not necessary to develop to the correct flow characteristics because this analysis only seeks to approximate the loading applied to the turbine component. The undeveloped flow from the inlet will yield useful results.

The meshing of this volume in necessary to input the problem to the CFD solver. The meshing and CFD solver are both completed within the ANSYS workbench. The meshing is completed by the mechanical software within ANSYS and CFD solving is completed by the Fluent software within ANSYS. These softwares are commonly used in industry and are capable of achieving accurate results when used with significant attention to detail. The analysis completed for this research and development of the MTRT will be preliminary to allow the design process to advance into prototype manufacturing and testing. Future work should include a full CFD analysis of the system with attention to turbine geometry optimization for efficiency and flow domain characteristics.

4.1.2 Meshing

The method for meshing the volume of fluid in CFD is highly important and there should be grid independence in CFD simulation. In the CFD analysis of the MTRT, 4 meshes were generated to compare the effect of mesh size and quantity on the results of the CFD simulation. The quantity of elements used in the grid independence study range from 0.26 million to 3.1 million. The meshes are shown in FIGURE 4-2.

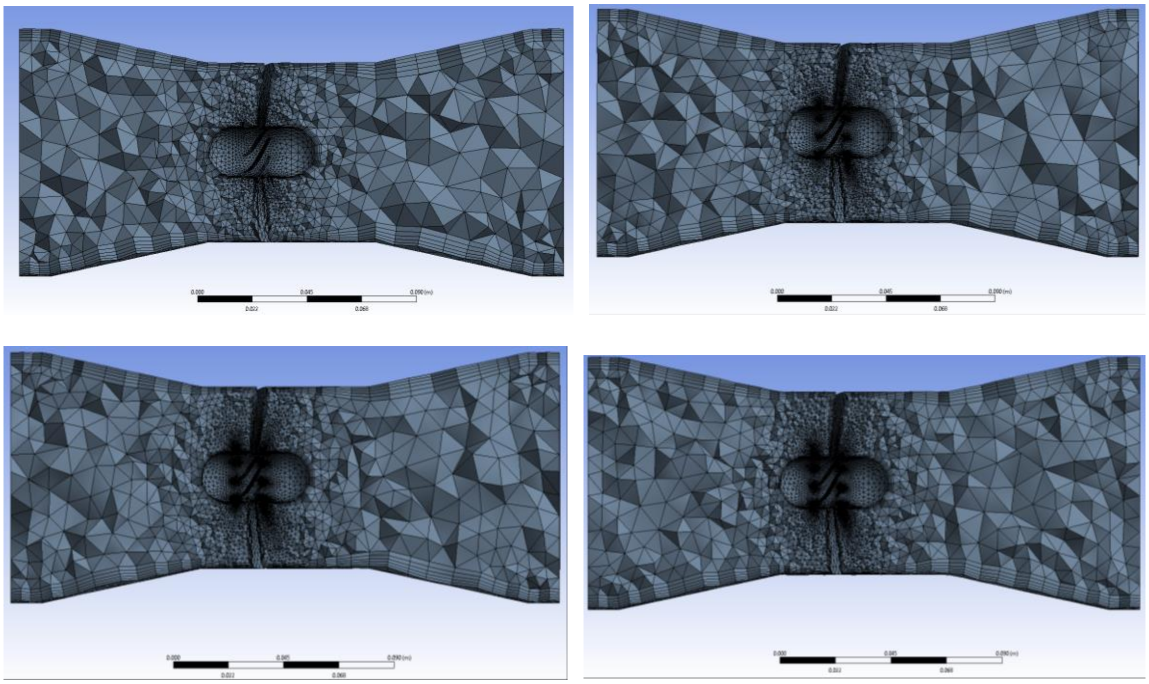

FIGURE 4-2: Varying mesh sizes used in grid independence study. 0.1 m (top left) to 0.0075 m (bottom right)

The various meshes shown in FIGURE 4-2 all include inflations around all the walls within the volume of fluid. The significant difference in mesh size is apparent around the turbine walls which is the area of importance in FPL simulations. In completing a grid independence study, reducing mesh size should affect the results of the simulation up to a certain size. When a reduction in mesh size yields no change to the simulation results, grid independence is achieved. To reduce computation time, the largest mesh size to achieve results unaffected by mesh size should be used. This grid independence study uses an inlet velocity of 10 m/s to amplify the flow parameters for studying the effect of mesh size. Grid independence will translate to less intense inlet flow conditions which will be used in the following FPL simulation. TABLE 4-1 shows the results of the grid independence study.

TABLE 4-1: Grid independence study results

Element Quantity	Max. Element Size (m)	Curvature Min. Element size (m)	Average Turbine Y+	Turbine Moment (Nm)	Average Turbine Pressure (Pa)	Mass Flow In (kg/s)	Mass Flow Out (kg/s)
261229	0.1	0.001	174.6	-102.9	1034939.3	80.797	80.797
1201154	0.025	0.00025	76.5	-106.1	1038248.0	80.797	80.801
2815161	0.01	0.0001	49.6	-103.9	1006383.3	80.797	80.797
3198734	0.0075	0.000075	46.6	-104.7	1006436.3	80.797	80.797

From TABLE 4-1, it can be observed that the reduction in element size from 0.01 m to 0.0075 m yields little change in CFD results. From the study, it can be concluded that the selection of a maximum element size of 0.01 m and a curvature minimum element size of 0.0001 m is sufficient to achieve accurate results.

4.1.3 Hydrodynamic Analysis

The fluid structure interaction is completed to output the static pressure on the turbine components to the mechanical analysis. In this case, the turbine is fixed in position which is comparable to the worst-case scenario of the turbine loading while in operation. The CFD solver uses the methods explained in section 2.2 to solve for the hydrodynamic variables. To do this in Fluent with a given mesh, the following set-up parameters were selected; see TABLE 4-2.

TABLE 4-2: Fluent set-up parameters

Parameter	Selection
Solver Type	Pressure-Based
Time	Steady-state
Viscous Model	k-omega SST
Material	Liquid Water
Inlet Velocity	0.778 m/s (100 GPM)
Inlet Turbulence	5%
Outlet Pressure	0 Pa Gage
Outlet Turbulence	20%
Hydraulic Diameter	0.1016 m
Initialization	Hybrid
Pressure-velocity Coupling Scheme	Coupled

Spatial Discretization	All Second Order Upwind

TABLE 4-2 shows the set-up parameters that were chosen for the CFD analysis. Values not displayed used the default Fluent values which are sufficient for this FPL simulation. The analysis was initialized with the hybrid method and solved with approximately 440 iterations. The values of the residuals in the analysis can be seen in the following figure, FIGURE 4-3.

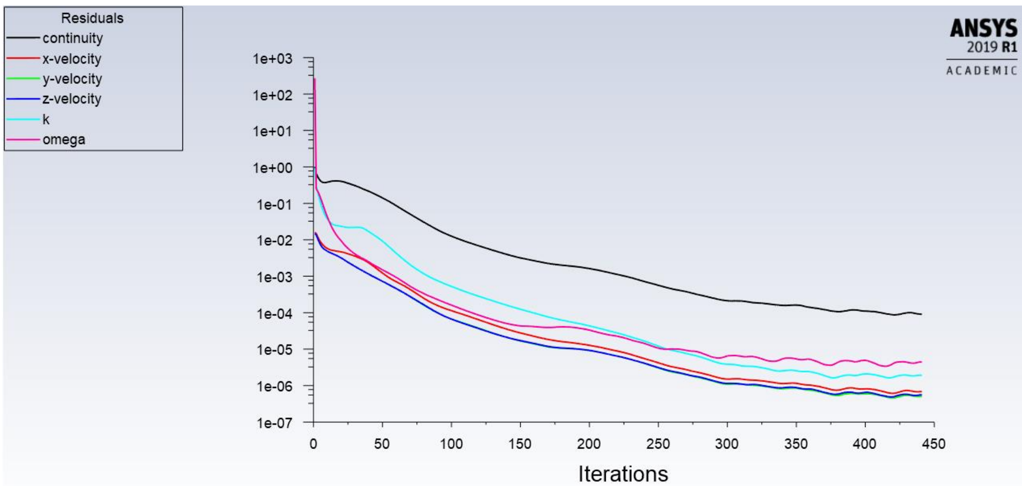

FIGURE 4-3: Plot of residuals from ANSYS Fluent CFD solver

It can be observed in FIGURE 4-3 that the variables in the CFD solver converge loosely. The standard for high convergence is 1e-6, however, 1e-4 is sufficient for preliminary analyses. Improvements to convergence require finer mesh which require computational resources that are unavailable and impractical for this analysis. The results from the CFD solver yield useful information such as the static pressure on the turbine components. The contour of this static pressure can be seen in the following figure, FIGURE 4-4.

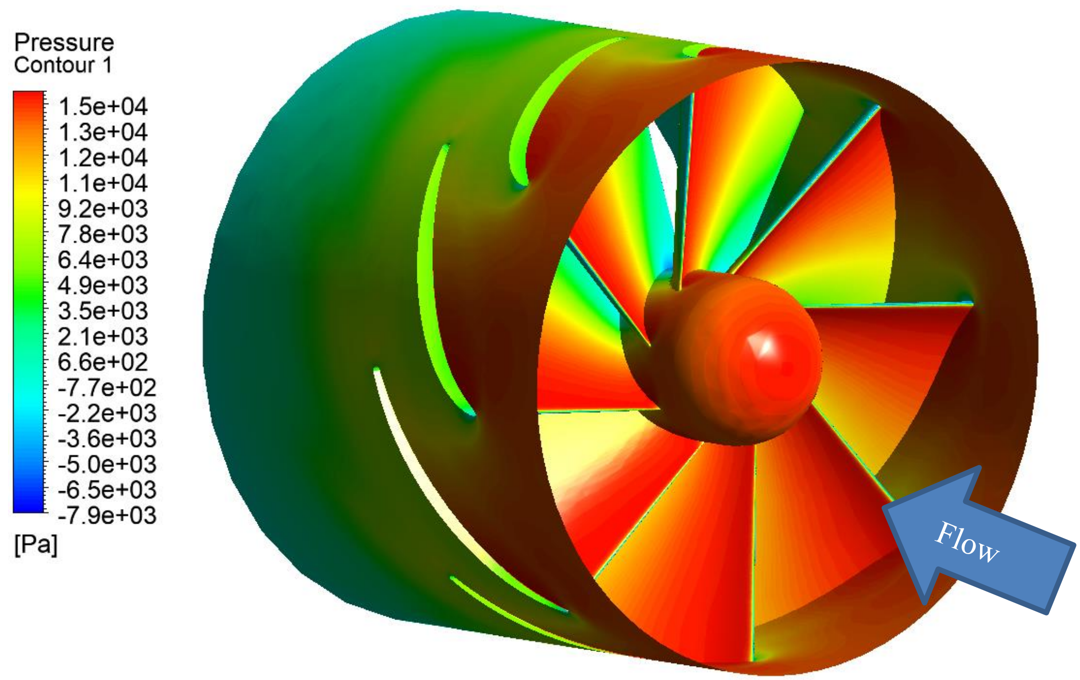

FIGURE 4-4: Contour plot of static pressure on turbine components

As expected, in FIGURE 4-4 the turbine blades are showing high pressure on the up-stream side and low pressure on the down-stream side. This is what causes the lift that causes the turbine to rotate. The static pressure from the FPL simulation can be integrated over the surface area of the blade to obtain to non-rotational torque. This value was calculated by Fluent to be 0.66 Nm. This figure also shows the pressures that will be imported into the mechanical analysis.

The following figure shows the contour of velocity through the center of the conduit and the turbine; see FIGURE 4-5.

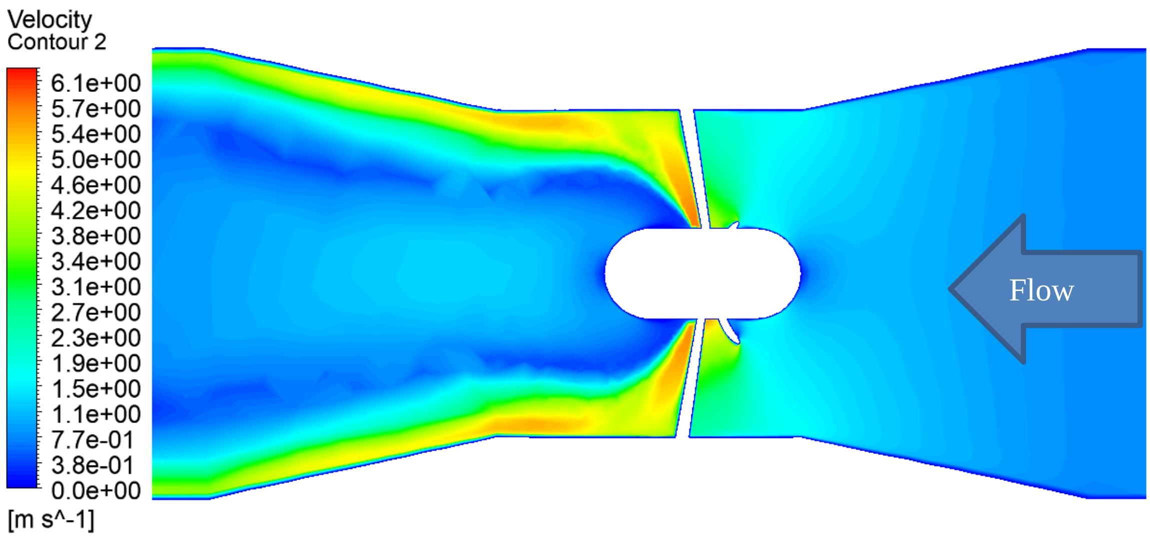

FIGURE 4-5: Contour plot of water velocity magnitude in center of conduit

In FIGURE 4-5 it can be observed that the turbine blades are constricting the water flow and inducing turbulence which raises the velocity of the water down-stream of the turbine blades. It can also be seen that there is a vortex behind the turbine with very low velocities. The spiraling flow down-stream of the turbine can be seen in the following figure, FIGURE 4-6.

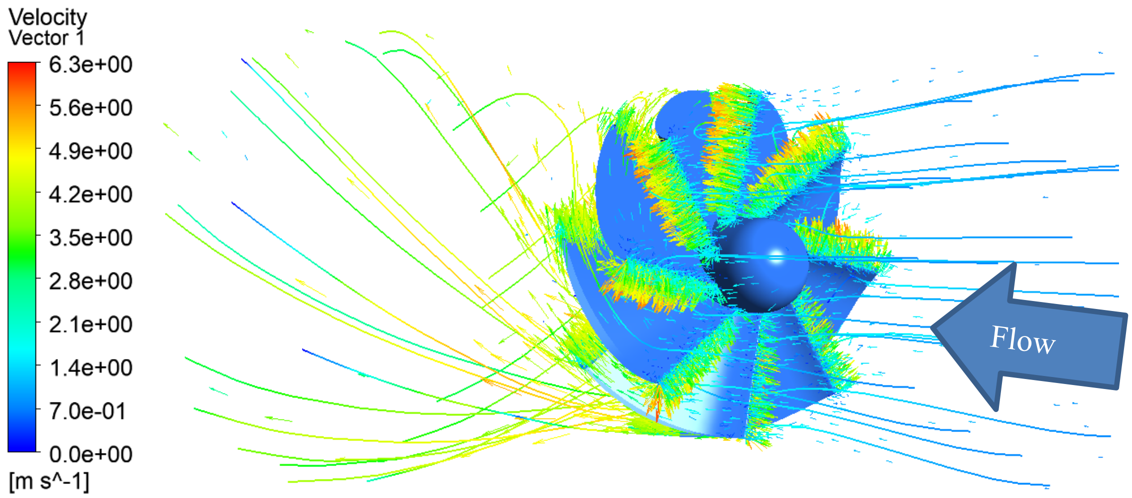

FIGURE 4-6: Velocity streamlines and vectors through volume of fluid

It is observable in FIGURE 4-6 that the turbine blades constrict the water which increases the velocity. The velocity is greatest at the leading edge of the turbine blade which is to be expected. This interaction between the leading edge and the water will likely cause erosion that will need to be considered in the further development of the turbine component. The prototype development will continue with rapid prototype material turbine blades which would be likely to erode in long term use.

4.1.4 Conclusion

The CFD analysis is necessary to determine the loading on the turbine component. The static pressures applied the turbine surfaces will be imported into the mechanical analysis described in section 4.3. Although the results are preliminary, the loads determined by the CFD simulation will be of use for determining if the turbine component is capable of withstanding the anticipated loads that will be applied in testing and eventually in operation. Future work should include the iterative design changes of the turbine geometry to improve efficiency with respect to the flow characteristics of the intended site.

4.2 Magnetostatic Analysis

4.2.1 Problem Definition

The magnetostatic analysis is necessary to determine the torque transmission capabilities of the magnetic coupling. The operation for determining this limit is to determine the torque as a function of the angular offset from equilibrium in the magnetic transmission. The selected software to solve Maxwell's equations and to determine this torque in post processing is Finite Element Magnetics Method (FEMM) software released by Dr. David Meeker [38]. The analysis also warrants comparing different yoke materials to obtain the highest torque transmission capabilities. The comparison will include polylactic acid (PLA) plastic, iron-infused PLA plastic, and low-carbon steel as yoke materials, all of which have different magnetic permeabilities which affects the magnetic coupling torque capabilities. In manufacturing, the simple plastic is the cheapest option due to the availability of low-cost 3D printing. The iron-infused PLA is also a 3D printable material, however, the material cost is greater than standard PLA. Low-carbon steel has the most difficulties associated with manufacturing and is not a viable solution for the prototype development but will still be used in the analysis to allow for a better comparison between the material options and for future research.

The isotropic magnetic permeability is the parameter of interest in the yoke material and the values are well documented for common materials. TABLE 4-3 shows a comparison between the magnetic permeabilities of the material in question.

TABLE 4-3: Comparison of magnetic coupling yoke magnetic permeability

Material	Relative Magnetic Permeability (μ_o)	Source
PLA Plastic	1	[38]
Iron-infused PLA Plastic	5-8	[41]
Low-Carbon Steel (1018)	529	[38]

From TABLE 4-3, it can be observed that the PLA plastic has a permeability of 1 meaning it is equally as permeable as air. Iron-infused PLA has a permeability ranging from 5 to 8 with the variance most likely due to manufacturing inconsistencies. A mean value of 6.5 will be used in this analysis. Low-carbon steel has a permeability of 529 which means it is very magnetic.

To compare the materials, a consistent geometry representing a 2D cross-section of the magnetic coupling was used. The following geometry in FIGURE 4-7 was used in the FEMM problem set-up.

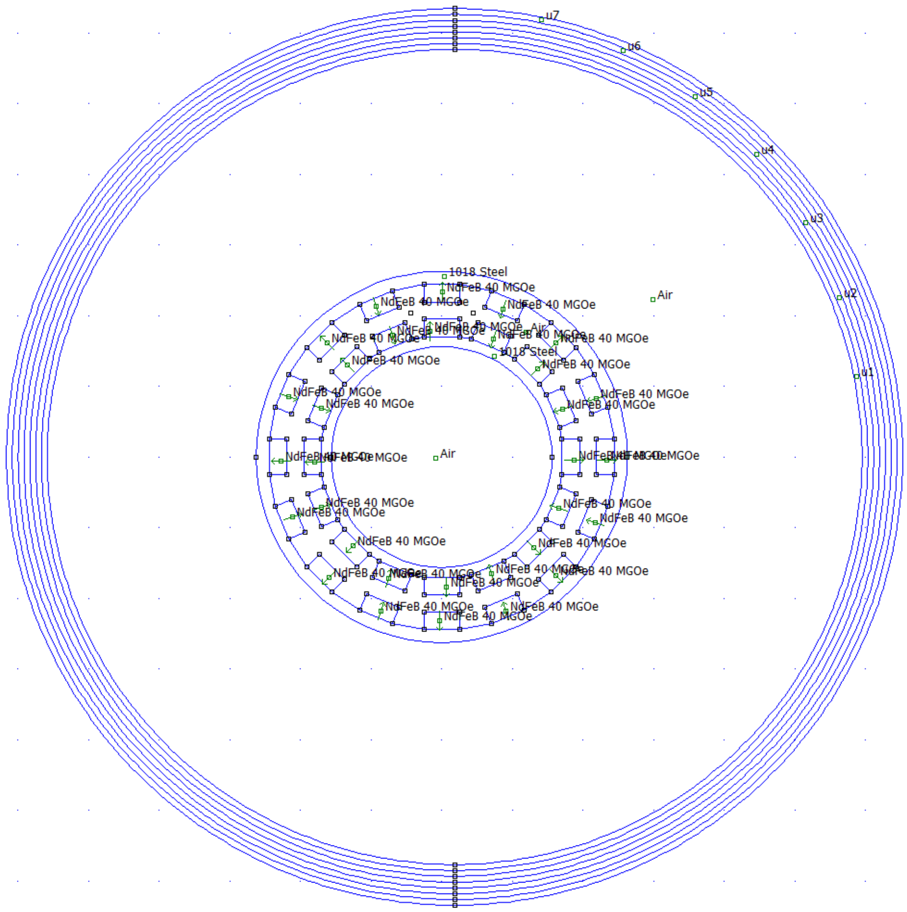

FIGURE 4-7: FEMM problem set-up

This figure contains the geometry used in the analysis. It contains the permanent magnets, the air gap, which includes the non-magnetic pipe, and the yokes of the inner and outer rotors. The permanent magnets used in the simulation are Neodymium (NdFeB) with a grade of 40 MGOe which is approximately the strength of the permanent magnets used in the mechanical design of the MTRT [42]. The magnetization curve of the selected magnets is shown in the following figure, FIGURE 4-8.

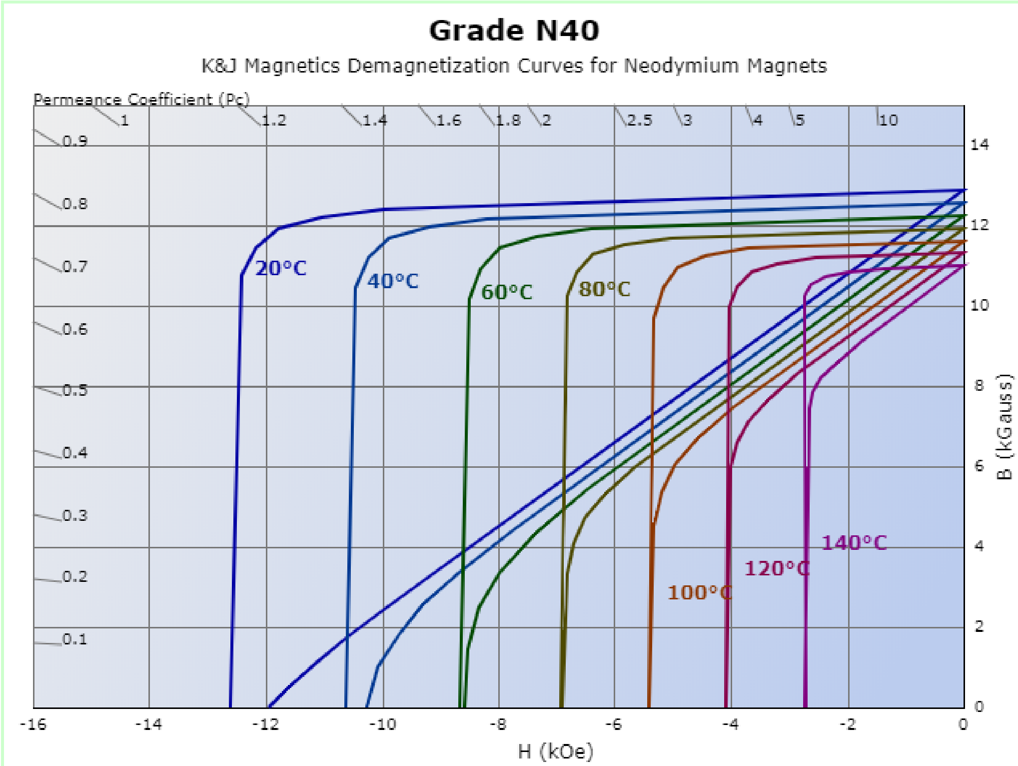

FIGURE 4-8: BH Curve of N40 Neodymium Magnet [42]

FIGURE 4-8 describes the BH curve of the permanent magnets which defines how the permanent magnet holds energy. The information of the BH curve is held within the FEMM software and used in the simulation. The magnetostatic problem is defined as planar with an axial distance of 1.5 inches, which is the length of the permanent magnets, and a default solver precision of 1e-8 is used as a stopping point for the linear solver. FEMM determines the material and other area specific properties with block labels. The permanent magnet blocks have a specified magnet strength and direction of polarity. The other blocks are mainly used to specify boundaries and permeability. The problem set-up also includes an open-boundary condition on the outside of the coupling which allows the simulation to solve the magnetics for a system in open air.

4.2.2 Meshing

The solver in FEMM uses a 2D mesh to complete the finite element simulation of the magnetics. FEMM automatically selects the mesh size but to validate the mesh size, a grid independence study is needed. The automatic mesh is shown below in FIGURE 4-9.

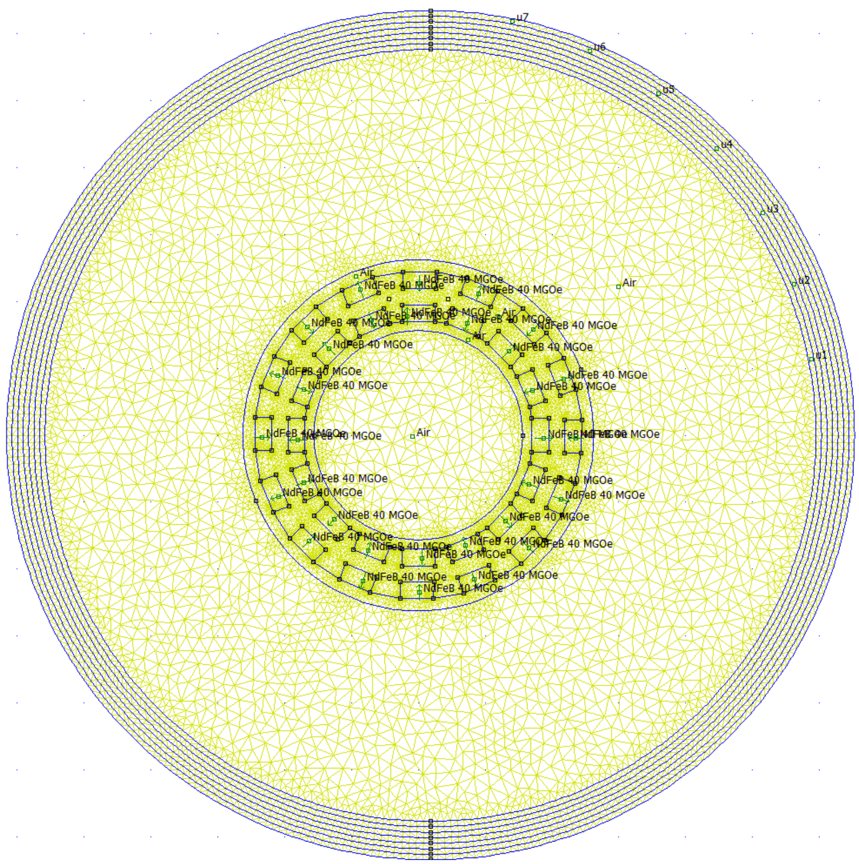

FIGURE 4-9: Meshing of problem in FEMM

An important aspect of magnetic simulation is the mesh size in areas of importance. In magnetostatic analysis of magnetic machines, the key interactions are occurring in the air gap between the rotors. The air gap is where the permanent magnet fields are interacting to cause the torque transmission in the coupling. To determine the effect of varied mesh size in the air gap region in the simulation, a grid independence study with varied mesh sizes was completed. FIGURE 4-10 shows a visual representation of the varied mesh sizes in the air gap.

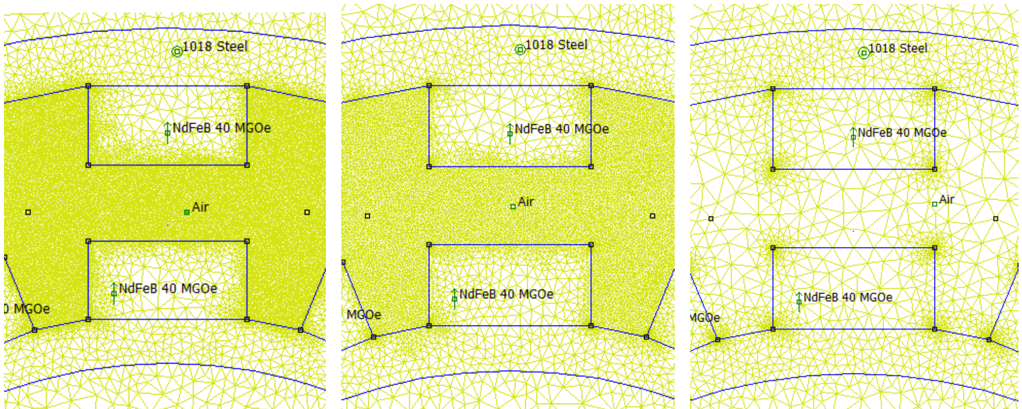

FIGURE 4-10: Comparison of air gap mesh sizes. 0.005 in (left), 0.01 in (middle) and 0.1 in automatic size (right).

In FIGURE 4-10, it is observable that the mesh size is varying in the air gap. The meshing scripting also creates tapering elements of similar size elements in the regions that are adjacent to the air gap to allow for size matching between the regions. The results of the grid independence study are shown in FIGURE 4-11.

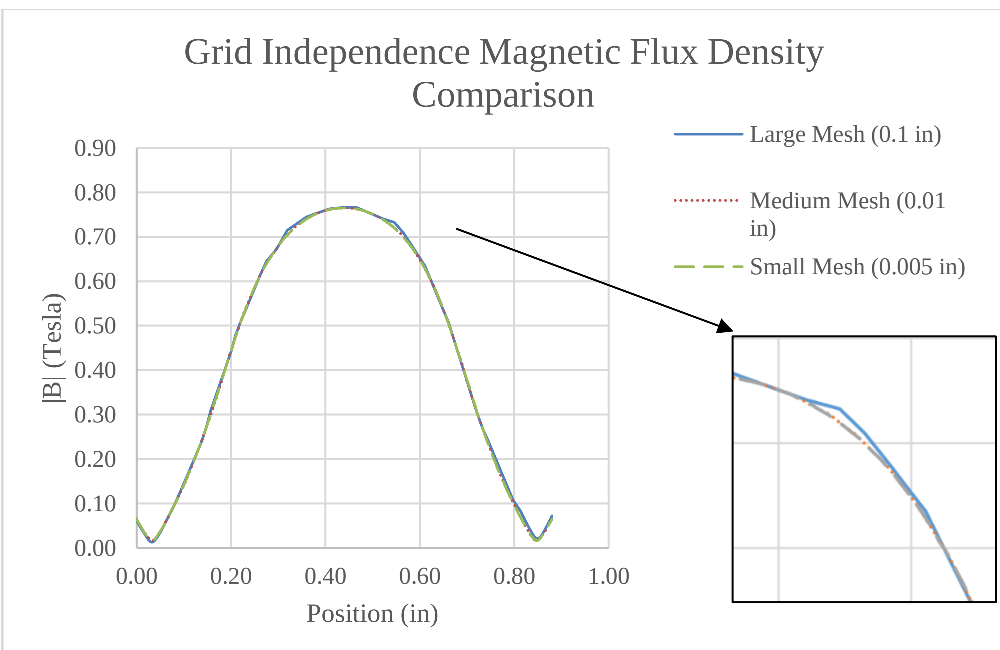

FIGURE 4-11: Magnetostatic grid independence

In FIGURE 4-11 a comparison in the flux density ($|B|$) in an arbitrary location within the air gap (see FIGURE 4-13) was completed. The computation times of one iteration of solving for the large, medium and small mesh were 13 seconds, 54 seconds and 270 seconds respectively. From the results it can be concluded that the large mesh caused inconsistencies in the profile of the flux density that are observable through the bumps in the curve. The small and medium mesh lack this inconsistency and have a smooth profile of flux density that is to be expected. The overlapping of the small and medium profiles leads to the conclusion that the refining of the mesh size from 0.01 inches to 0.005 inches yields little to no improvements in simulation accuracy. In attempt to lower computational expense the medium mesh will be used in the following analysis.

4.2.3 Results

The results describe the comparison of the yoke material of the magnetic coupling for peak torque transmission. The comparison of flux density is shown in the following figure, FIGURE 4-12.

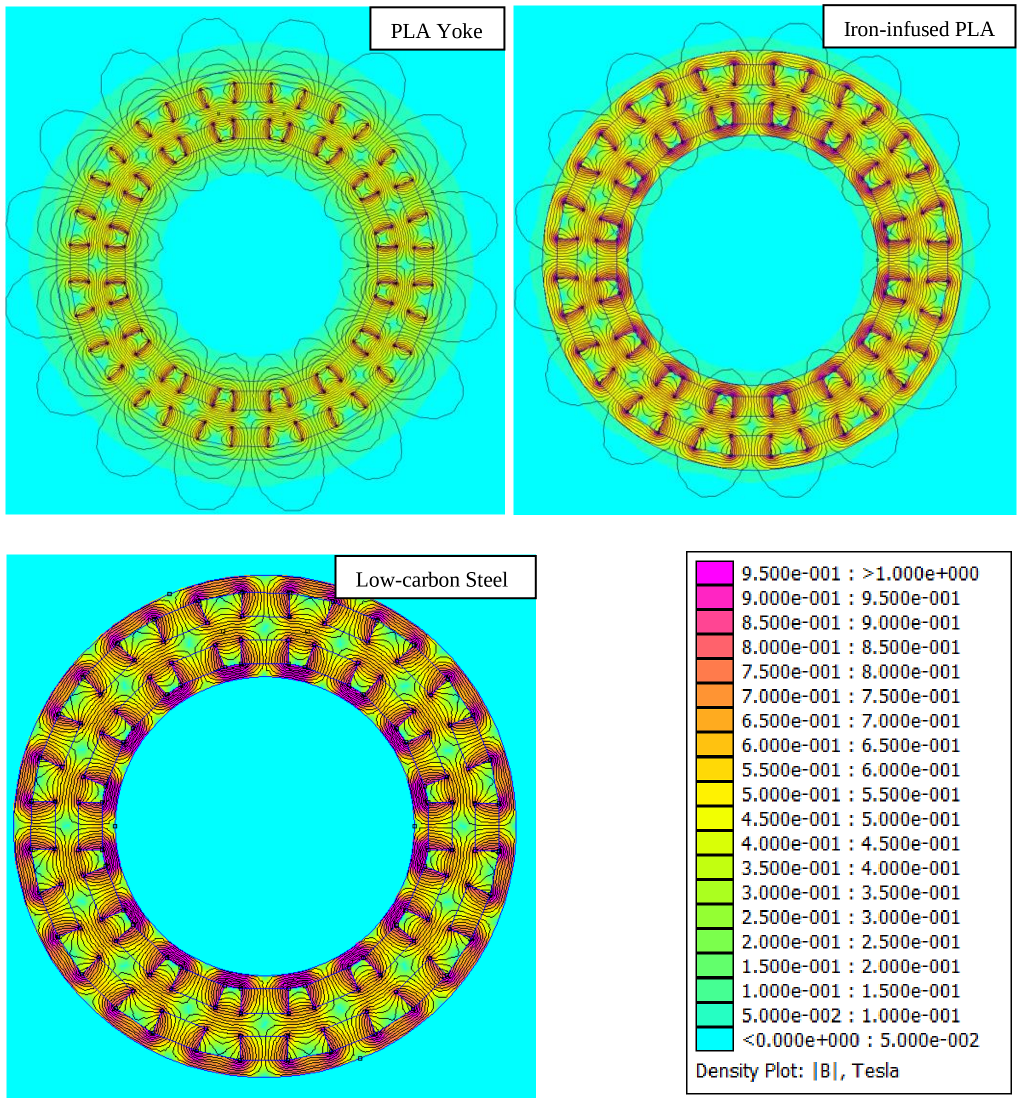

FIGURE 4-12: Yoke material flux lines and density comparison

It can be observed that the PLA yoke yields the lowest flux density and the low-carbon steel yields the highest flux density. Because the flux density related to the torque transmission capability, a comparison of flux density in the air-gap is necessary. An arbitrary line was selected in the air-gap for the comparison; see FIGURE 4-13.

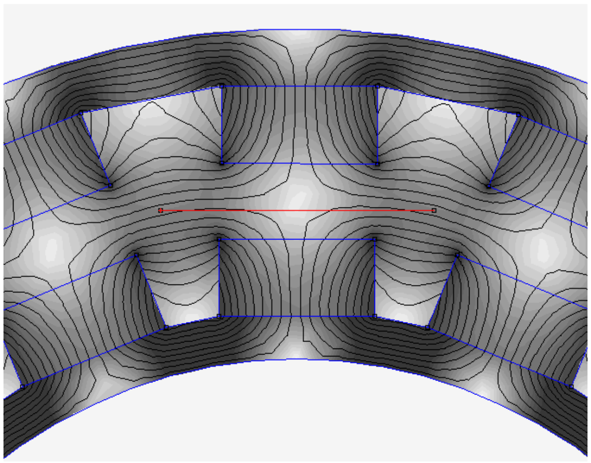

FIGURE 4-13: Arbitrary air-gap flux measurement location

This location, shown in FIGURE 4-13, was used in the comparison of air-gap flux density with different yoke materials. The comparison results are shown in the following figure, FIGURE 4-14.

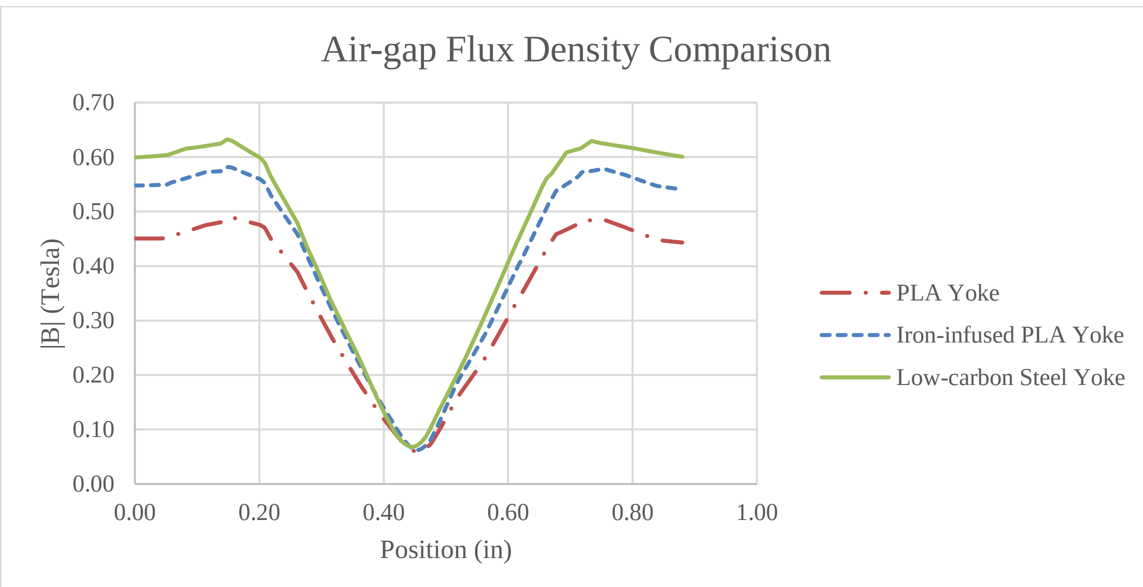

FIGURE 4-14: Air-gap flux density comparison

In FIGURE 4-14, it is observable that the PLA plastic yoke yields the lowest flux density and the low-carbon steel yoke yields the highest flux density. It can also be observed that the use of iron-infused PLA yields an increase in flux density in the air-gap compared to the standard PLA. This flux density analysis is followed with the peak torque analysis. With the methods described in section 2.3, the steady-state weighted stress tensor can be integrated over the permanent magnet area to get the torque value on the magnetic coupling rotor. The results of this analysis are shown in the following figure, FIGURE 4-15.

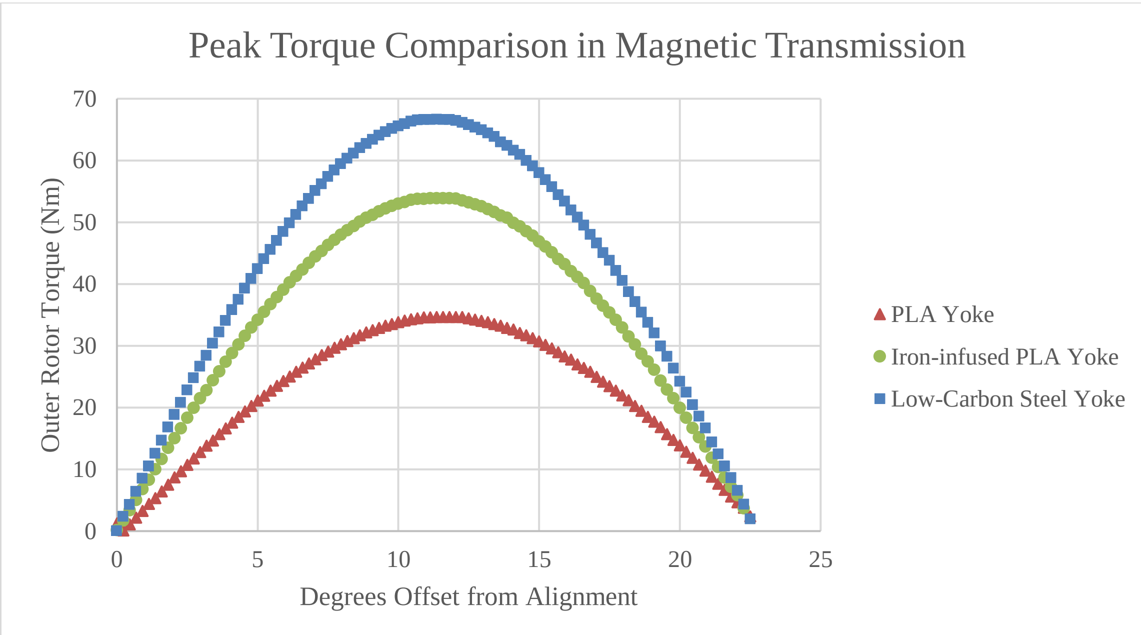

FIGURE 4-15: Magnetic coupling torque comparison

In FIGURE 4-15, it is observable that the PLA yoke yields the lowest torque transmission capability and the low-carbon steel yoke yields the highest torque transmission capability, as expected. Similar to the flux density comparison, the use of iron-infused PLA yields a significant improvement in torque transmission capability.

4.2.4 Conclusion

The design of the magnetic transmission yields torque transmission capabilities that are exceedingly high. In the prototype design and testing, there will be no torques applied to the turbine approaching the peak torque of the transmission due to the expected torque being on the order of 1 Nm from the FPL simulation. However, this analysis affirms that the use of a magnetic transmission yields very high torque transmission capabilities. It is suggested that in future design, the use of permanent magnet be limited to the minimum necessary to transmit the expected load of the system. Minimizing the permanent magnet mass will lower cost and enable the slipping of the poles in peak torque conditions to protect the components of the system from overloading. Also, the use of permeable yoke materials will increase the torque transmission capabilities, therefore the magnetic mass can be decreased, and manufacturing cost can be lowered. The development of the prototype will use non-permeable PLA plastic to allow the testing to move forward.

4.3 Mechanical Analysis

4.3.1 Problem Definition

The mechanical analysis is necessary to ensure the components within the system are structurally robust enough to withstand the forces that are present. Having structurally robust components is necessary to reduce the cost associated with maintenance and repair. The mechanical analysis completed for the prototype design of the MTRT involves the turbine component which converts the hydrokinetic energy into rotational energy in the powerplant and the inner and outer rotor which are the structural components in the magnetic transmission. There will also be consideration to the load carrying purchased components in the system which are the belt and the bearings. All of the manufactured components are subjected to considerable loading and have a high cost of repair. This mechanical analysis serves the purpose of advancing the development of the prototype and the methods can be used in the scaling up of the design.

It is necessary to define the load path through the system and identify the components that are subject to loading. The load path of critical components identified is shown in the following figure.

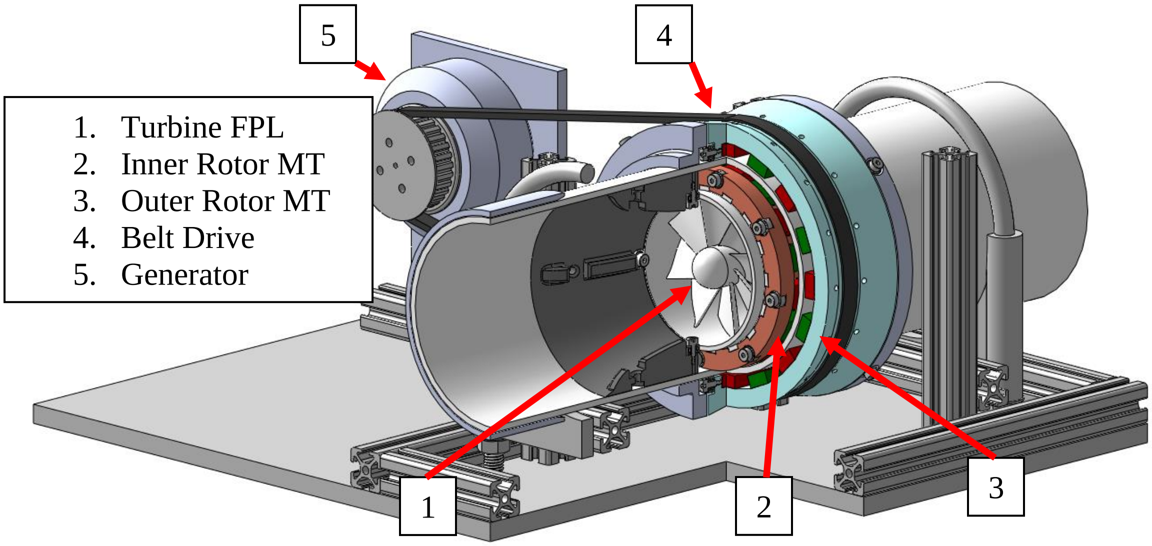

FIGURE 4-16: System mechanical load path

As shown in FIGURE 4-16, the load path begins at the FPL on the turbine from the water, and continues through the magnetic transmission, the belt and the generator components. The mechanical analysis will consider each of the components that are included in the load path. The components that are custom to the MTRT will be manufactured with rapid prototype 3D printing. The machine used to print the components will be a 3D Systems ProJet Printer. The parts will be printed with the VisiJet M3 Crystal thermoset plastic. Being a UV cured resin 3D printing process similar to SLA, the final material can be assumed to be isotropic. The neodymium permanent magnets in the assembly will also have structural and inertial implications so the material properties are also needed. The material properties for the 3D printer plastic and the permanent magnets are shown in TABLE 4-4.

TABLE 4-4: Material properties for VisiJet M3 Crystal 3D printer plastic

Property	Value
VisiJet M3 Crystal [43]	
Color	Clear
Density	1.02 g/cm^3
Tensile Strength	42.4 MPa
Tensile Modulus	1463 MPa
Poisson’s Ratio	0.35
Neodymium [42]	
Density	7.5 g/cm^3
Tensile Strength	80 MPa
Tensile Modulus	160 GPa
Poisson’s ratio	0.24

The expected loads for the MTRT were identified and are shown in the following table, TABLE 4-5.

TABLE 4-5: Loading parameters for mechanical analysis

Load	Value
Torque	40 Nm
Fluid Velocity	1.48 m/s (100 GPM)
Expected Tip Speed Ratio	6.5 [44]
Turbine Rotational Speed	261.2 rad/s (2494.2 RPM)

The torque value of 40 Nm was selected due to being slightly greater than the slipping torque of the magnetic transmission with a PLA yoke. Theoretically the torque in the system should not exceed this value. A fluid velocity of 100 GPM was selected due to it being a common flow rate of micro hydropower plants and the flow rate of the anticipated test location. From similar research presented by Nishi et al., a tip speed ratio of 6.5 was predicted for an axial turbine in an enshrouded flow [44]. This value was predicted for a 3-blade turbine which have higher tip speed ratios than 8 blade turbines. The use of 6.5 for the tip speed ratio will yield greater rotational speeds which will represent a worst-case scenario.

4.3.2 Fluid-structure Interaction Structural Analysis

The turbine used in the MTRT hydro powerplant is modular and easily installed and changed in the system. To ensure the turbine component can withstand the loading applied by the water flowing through the system, a fluid structure interaction analysis is needed. The geometry used to create the volume of fluid in the CFD analysis is what is used in the mechanical part of the FPL simulation. This geometry is shown in the following figure, FIGURE 4-17.

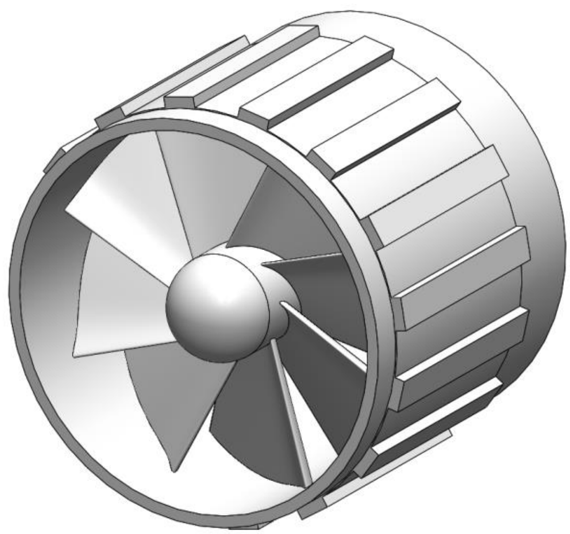

FIGURE 4-17: Turbine component model in SOLIDWORKS

The model shown in FIGURE 4-17 is imported into ANSYS Workbench where the results of the FPL CFD can be used to import the loads. The meshing of this component is completed in ANSYS Mechanical and shown in the following figure, FIGURE 4-18.

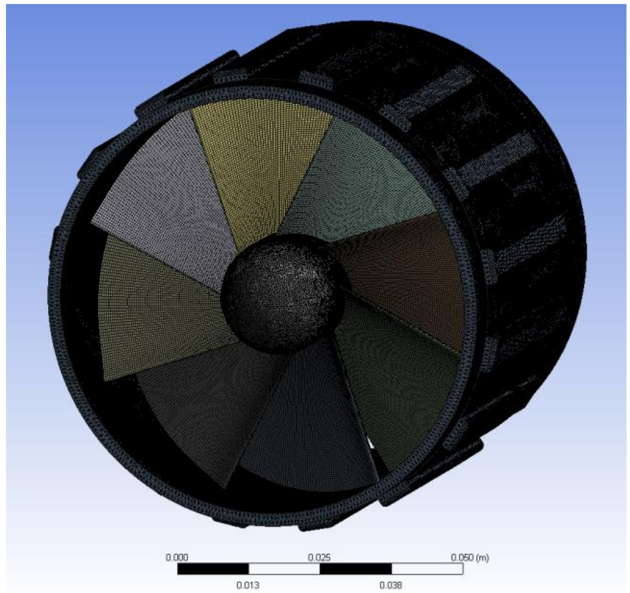

FIGURE 4-18: Turbine component mesh in ANSYS Mechanical

As shown in FIGURE 4-18, the turbine mesh uses a combination of tetrahedral and hexahedral elements. The grid independence was ensured based on the average von Mises stress in the model. The mesh was found to not affect the results up to a mesh size of 0.001 m however a 0.0004 m was selected due to minor differences in computational expense and more accurate CFD pressure importation.

The surface pressures that were calculated during the FPL CFD are imported to ANSYS Mechanical automatically through the Workbench connection. The importation averages the pressure on the CFD element surface and interpolates it for the mechanical element surface. The results of this importation are shown in the following figure, FIGURE 4-19.

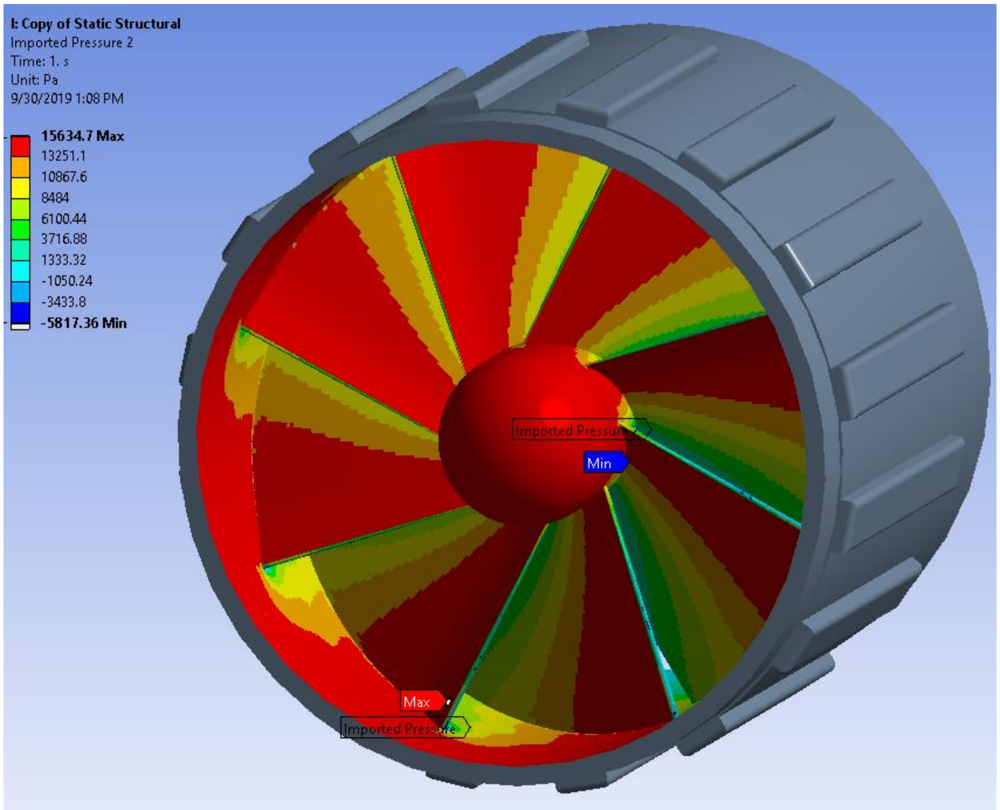

FIGURE 4-19: CFD static pressure from ANSYS Fluent

FIGURE 4-19 shows the imported pressure on the surfaces of the turbine component. The pressure is determined by the surface pressure of the FPL CFD which is shown in a contour plot in a previous section (FIGURE 4-4). The outer ring which interfaces with the inner rotor is defined as a fixed boundary condition. The turbine also has rotational inertia loads applied to include the stresses of the turbine rotating at high speeds (261.2 rad/s).

After running the mechanical simulation, the following results for equivalent (von Mises) stress are generated; see FIGURE 4-20.

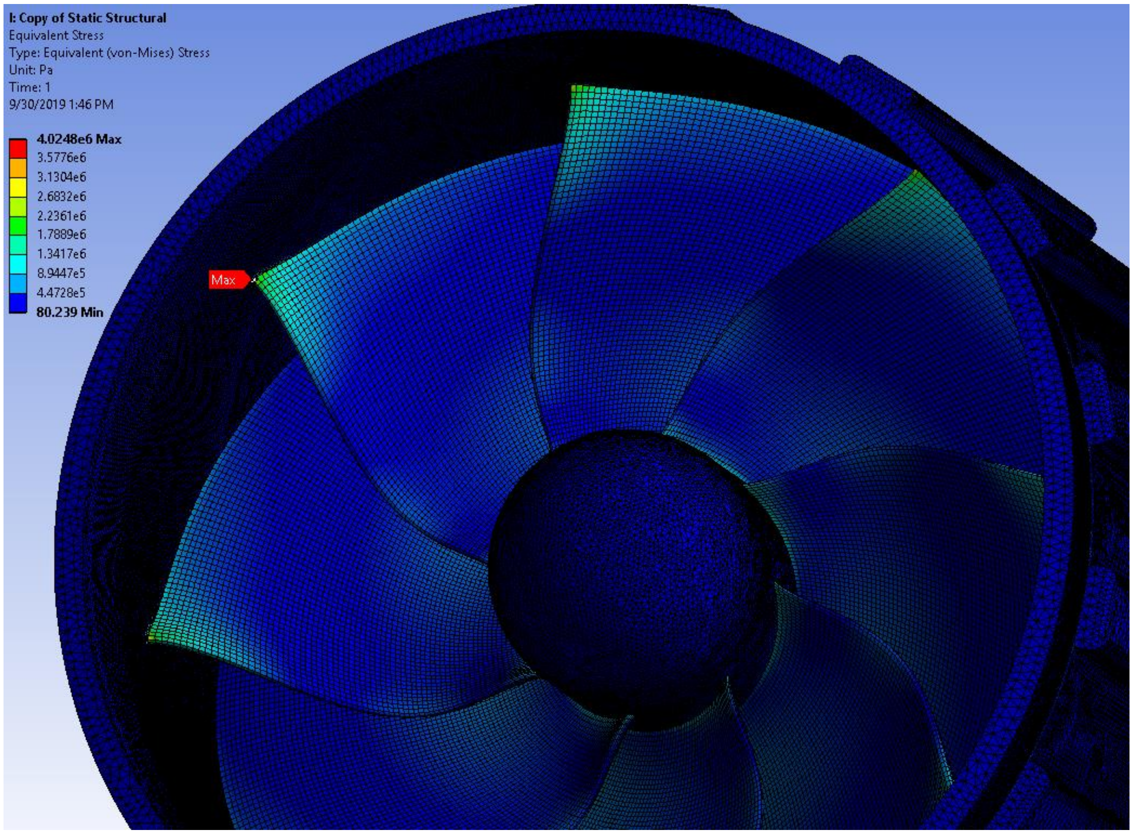

FIGURE 4-20: Turbine component equivalent stress

In FIGURE 4-20, it is apparent that the max equivalent stress is located on the leading edge of the turbine blade where the blade ring and the blade interface. Due to stress singularities, the stress at this location is higher than expected although still less than the yield strength of the turbine component material. The advertised yield strength of material is 42.4 MPa and the max equivalent stress is 4.1 MPa which equates to a factor of safety of 10.4. This safety factor is satisfactory for the MTRT prototype design and testing. The manufactured part is shown in the following figure, FIGURE 4-21.

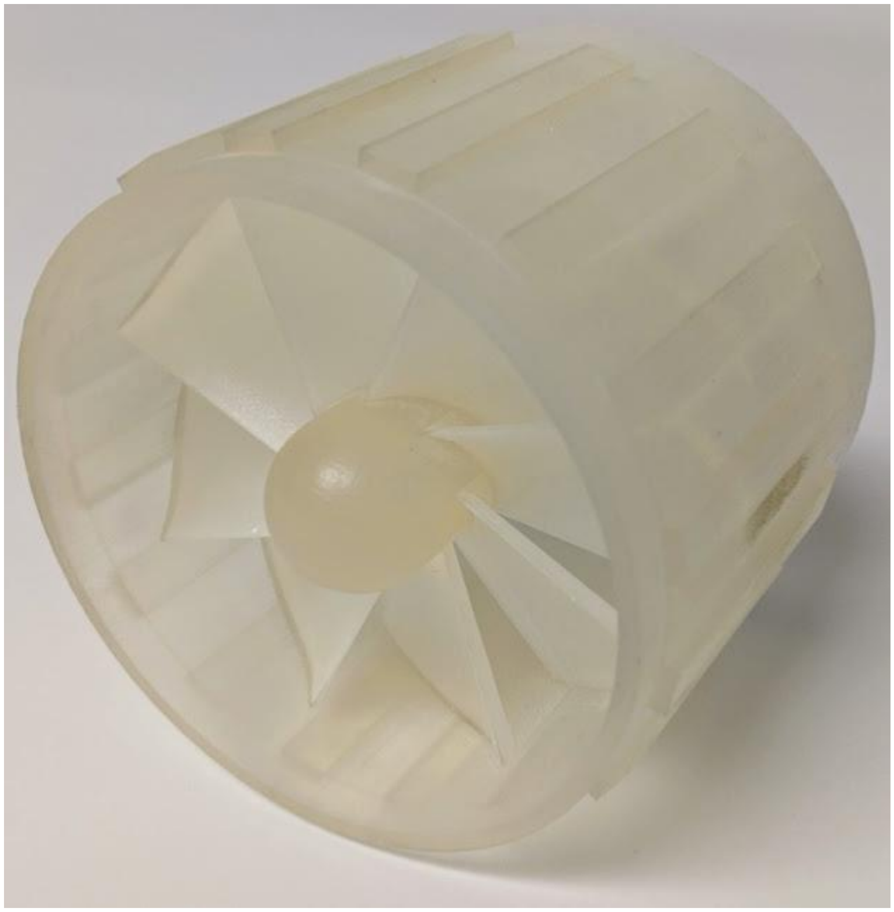

FIGURE 4-21: Final 3D printed turbine component

4.3.3 Magnetic Transmission Structural Analysis

To ensure that the structures holding the permanent magnets in the magnetic transmission can withstand the significant torques applied during testing and operation a structural analysis is necessary. The two structures are the inner and outer rotor and are manufactured with 3D printing out of the VisiJet M3 Crystal plastic material and include neodymium magnets. The inner rotor without the magnets is shown in the following figure, FIGURE 4-22.

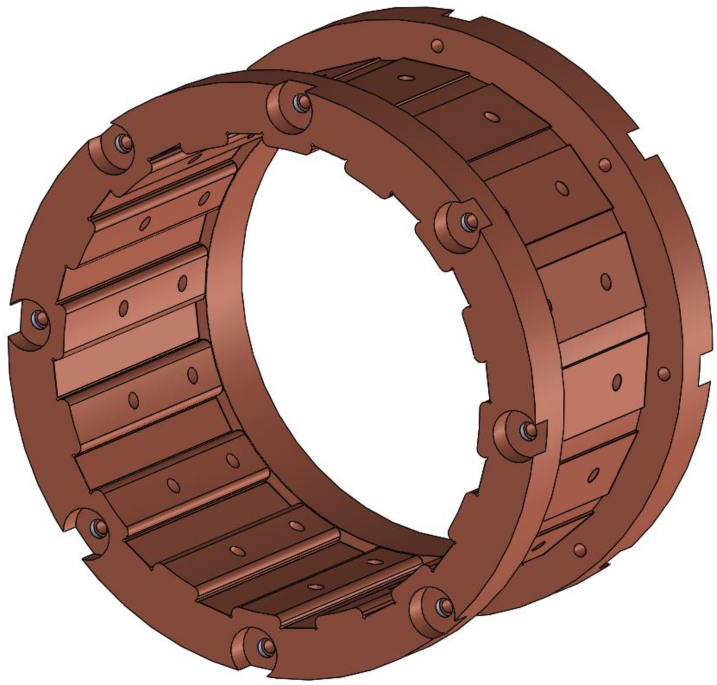

FIGURE 4-22: Inner rotor model in SOLIDWORKS

FIGURE 4-22 shows the inner rotor without the magnets modelled in SOLIDWORKS. In the meshing of this component and in the analysis the magnets will be included to add the inherent loading of inertia from rotating. The magnet density will drive the mass of the rotor and therefore the inertial loading. The mesh created in ANSYS Mechanical is shown in the following figure, FIGURE 4-23.

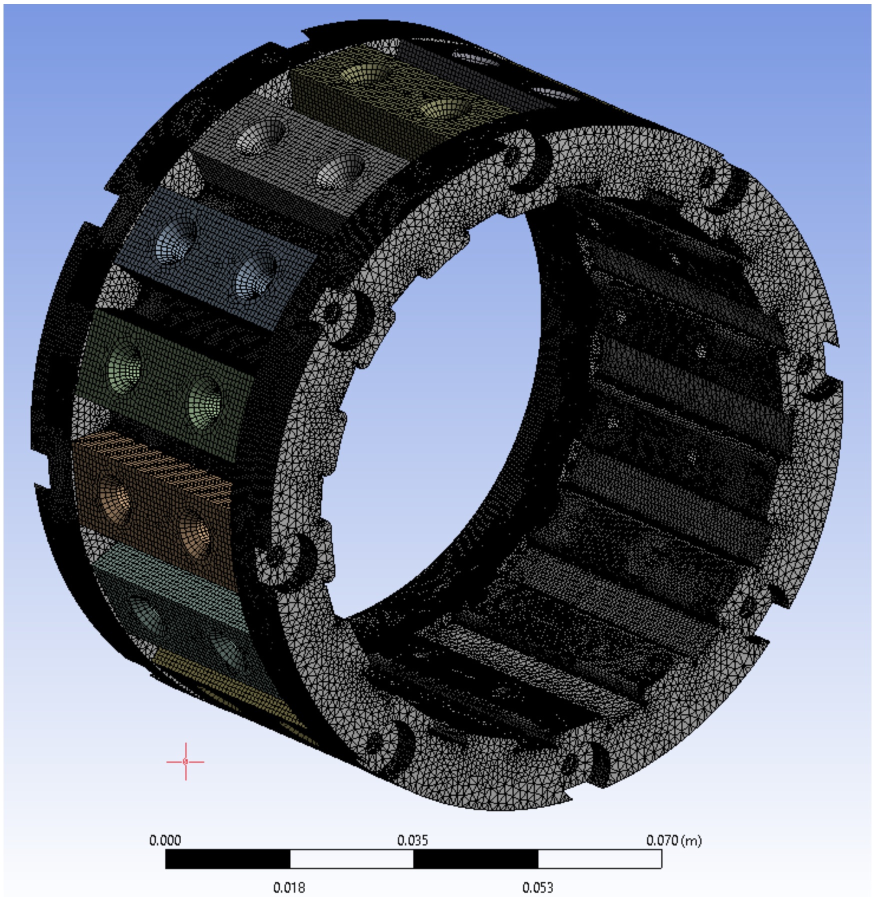

FIGURE 4-23: Inner rotor mesh

As shown in FIGURE 4-23, the inner rotor mesh uses a combination of tetrahedral and hexahedral elements. The grid independence was ensured based on the average von Mises stress in the model. The mesh was found to not affect the results up to a mesh size of 0.0016 m, however, a 0.0008 m was selected due to minor differences in computational expense. The boundary condition set-up for the inner rotor in ANSYS Mechanical is shown in the following figure, FIGURE 4-24.

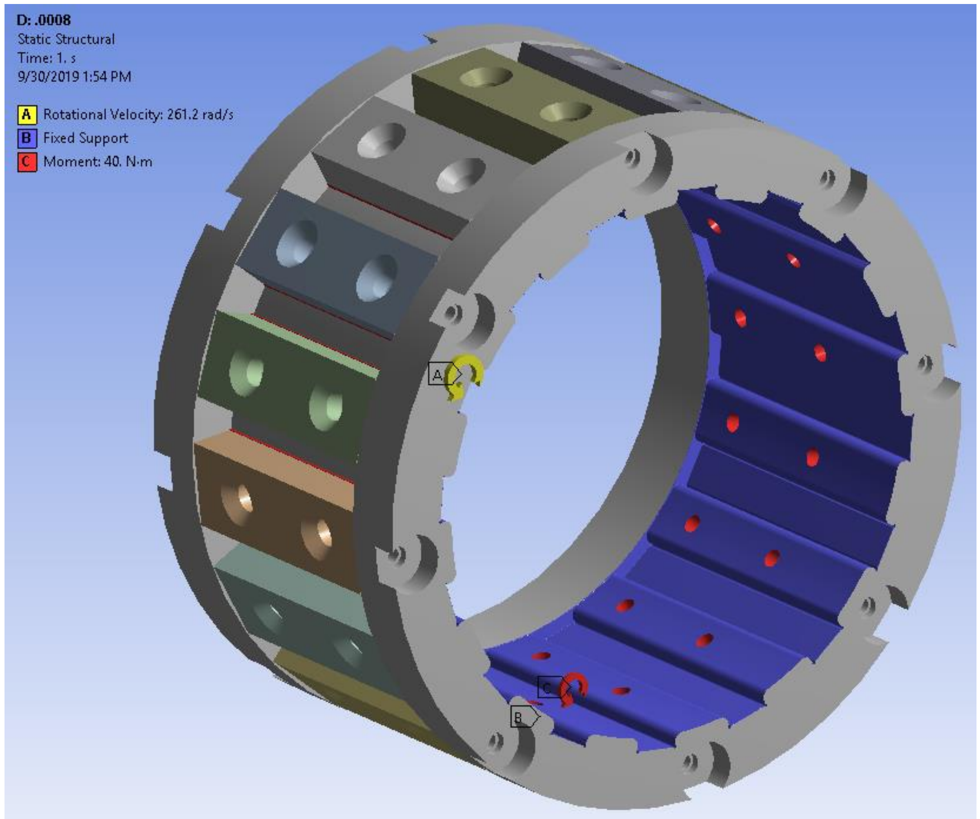

FIGURE 4-24: Inner rotor boundary conditions in ANSYS Mechanical

In FIGURE 4-24, it can be observed that the inner surface that interfaces with the turbine component is set as a fixed support, the moment of 40 Nm is applied to the screw holes and the surface where the magnets interface with the rotor. Also, a rotational speed of 261.2 rad/sec is applied to the inner rotor and the magnets. This set-up yields the following results for equivalent (von Mises) stress; see FIGURE 4-25

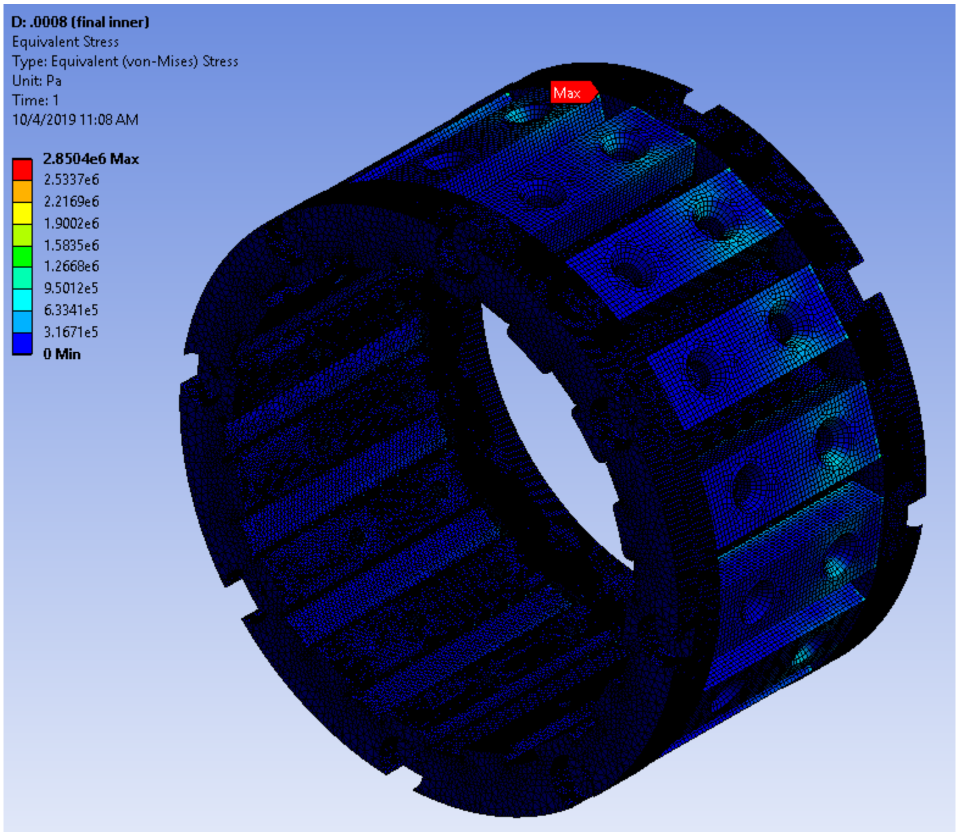

FIGURE 4-25: Inner rotor equivalent stress

FIGURE 4-25 shows the equivalent stress in the inner rotor from all the expected loads. There are also stress singularities present in this analysis, however, the stress is below the yield strength so the stress singularities that increase with mesh refinement can be justifiably ignored. The advertised yield strength of material is 42.4 MPa and the max equivalent stress is 2.85 MPa which equates to a factor of safety of 14.9. This safety factor is satisfactory for the MTRT prototype design and testing. The final assembled inner rotor with the turbine component is shown in the following figure, FIGURE 4-26

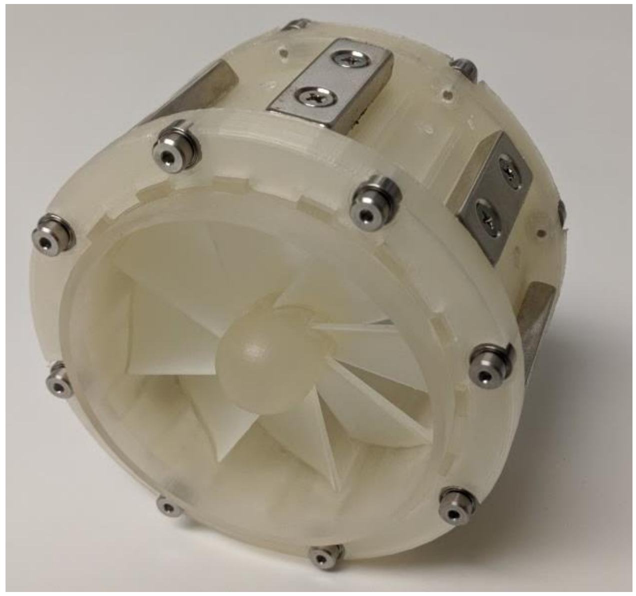

FIGURE 4-26: Assembled inner rotor with turbine component

The torque analysis also includes the simulation of the outer rotor in the magnetic transmission. The simulation of this rotor is very similar to the simulation of the inner rotor. The outer rotor model created in SOLIDWORKS is shown below in FIGURE 4-27.

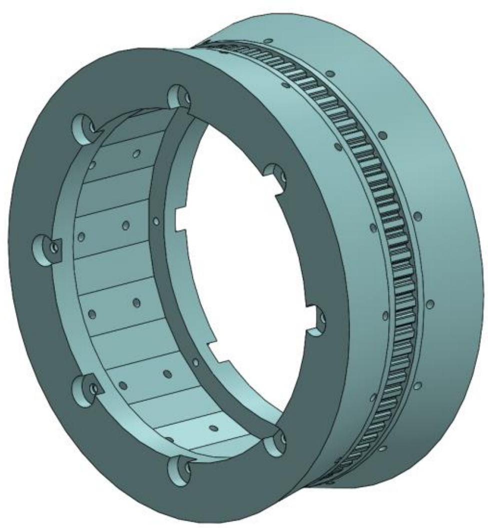

FIGURE 4-27: Outer rotor model in SOLIDWORKS

FIGURE 4-27 shows the outer rotor without the magnets modelled in SOLIDWORKS. In the meshing of this component and in the analysis the magnets will be included to add the inherent loading of inertial forces from rotating. The magnet density will drive the mass of the rotor and therefore the inertial loading. The mesh created in ANSYS Mechanical is shown in the following figure, FIGURE 4-28.

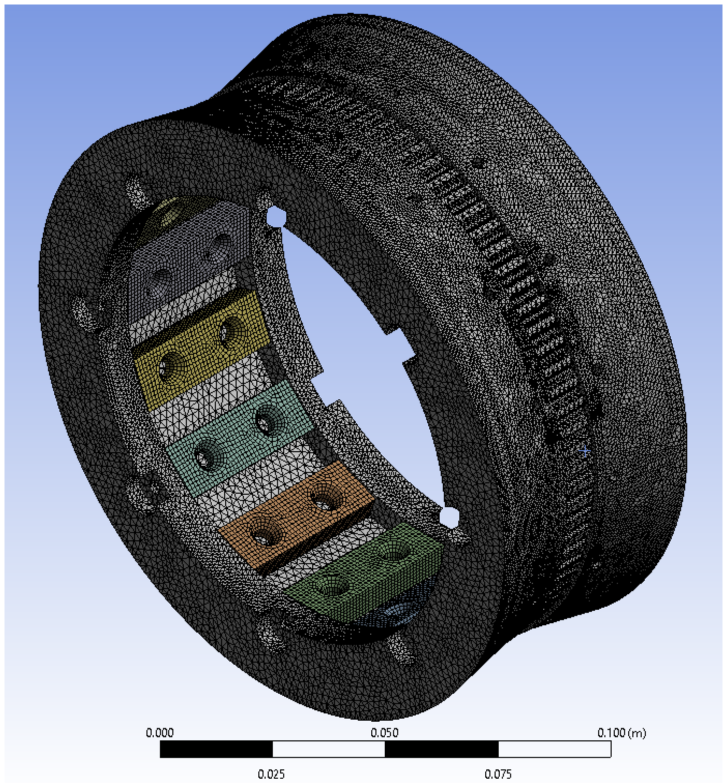

FIGURE 4-28: Outer rotor mesh in ANSYS Mechanical

As shown in FIGURE 4-28, the outer rotor mesh uses a combination of tetrahedral and hexahedral elements. The grid independence was ensured based on the average von Mises stress in the model. The mesh was found to not affect the results up to a mesh size of 0.0016 m, however, a 0.001 m was selected due to minor differences in computational expense. The boundary condition set-up for the inner rotor in ANSYS Mechanical is shown in the following figure, FIGURE 4-29.

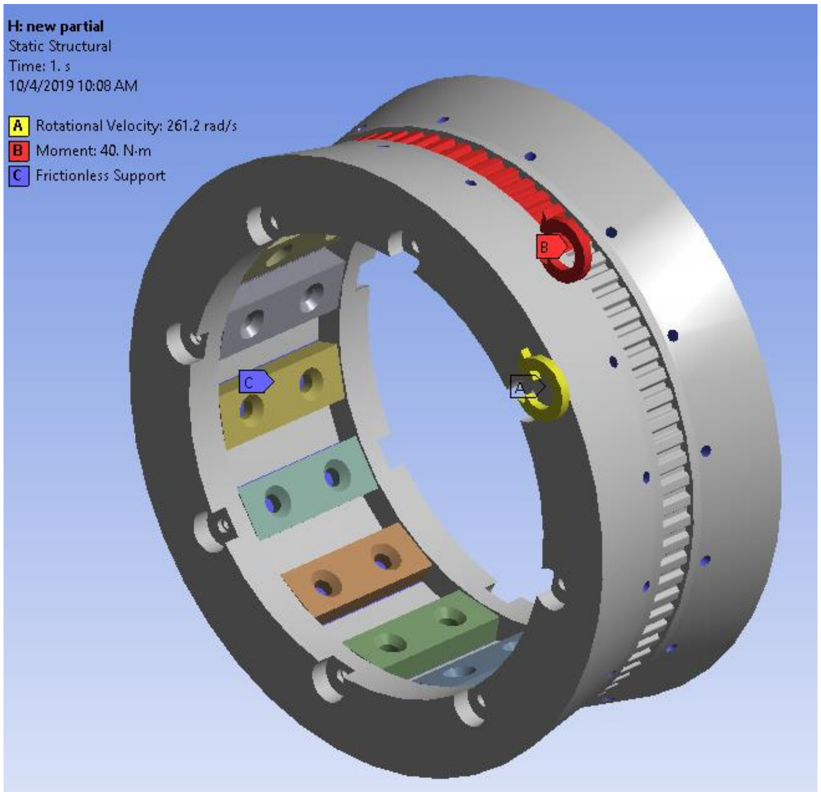

FIGURE 4-29: Outer rotor boundary conditions in ANSYS Mechanical

In FIGURE 4-29, it can be observed that the outer surface that interfaces with the belt drive (approximately 50/85 sprocket teeth) is loaded to a moment of 40 Nm and the frictionless support boundary condition is applied to the screw holes and the surface where the magnets interface with the rotor. Also, a rotational speed of 261.2 rad/sec is applied to the inner rotor and the magnets. These boundary conditions are optimal for matching the actual loading the component will see in operation. This set-up yields the following results for equivalent (von Mises) stress; see FIGURE 4-30.

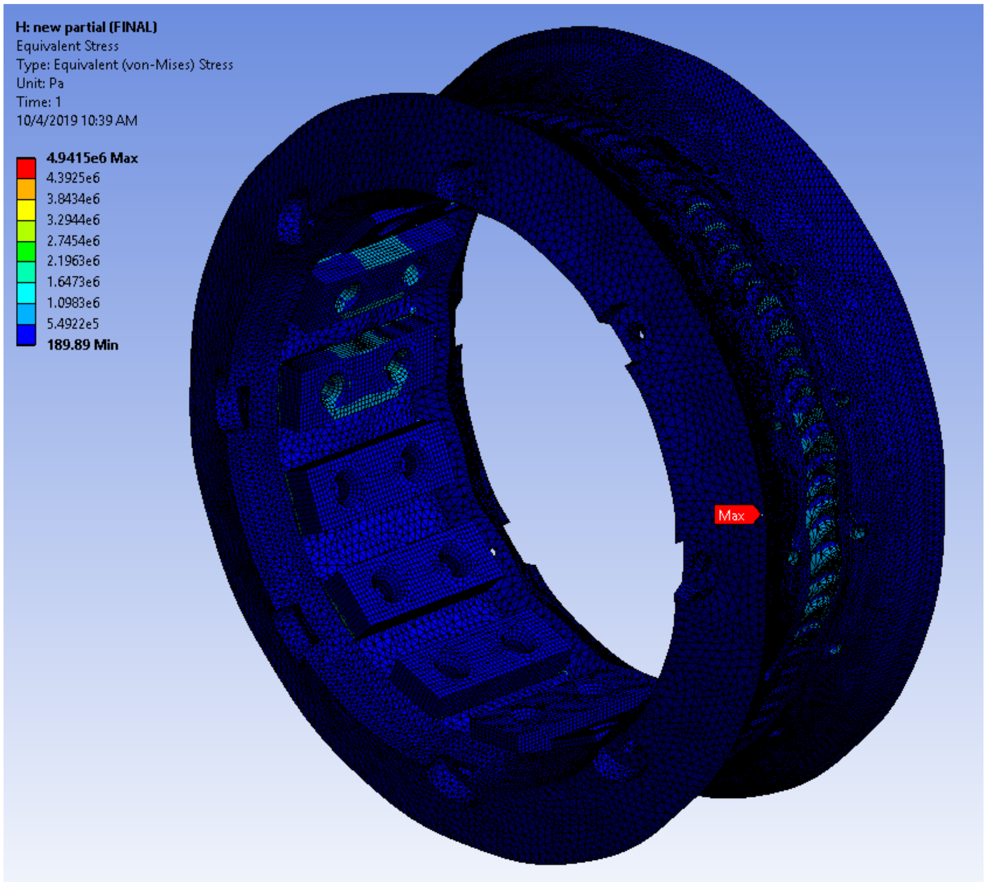

FIGURE 4-30: Outer rotor equivalent stress

FIGURE 4-30 shows the equivalent stress in the outer rotor from all the expected loads. There are also stress singularities present in this analysis, however, the stress is below the yield strength so the stress singularities that increase with mesh refinement can be justifiably ignored. The advertised yield strength of VisiJet material is 42.4 MPa and the max equivalent stress is 4.9 MPa which equates to a factor of safety of 8.7. This safety factor is satisfactory for the MTRT prototype design and testing. The assembled outer rotor is shown in the following figure, FIGURE 4-31.

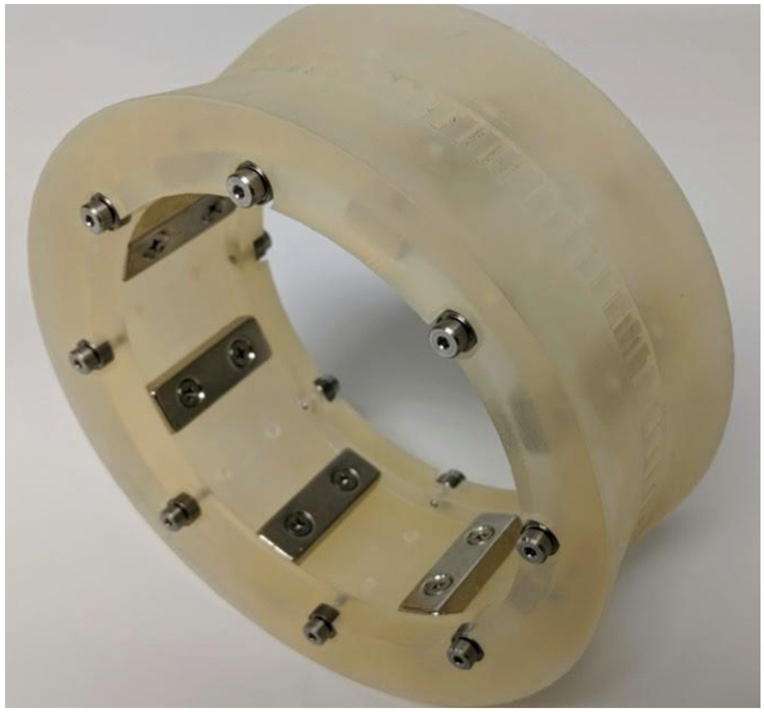

FIGURE 4-31: Assembled outer rotor

4.3.4 Standard Component Analysis

The design of the prototype MTRT requires the use of standard components purchased from the vendor McMaster-Carr. The belt, sprocket and bearings all need to withstand the expected loads during operation. The belt and sprocket analysis involves ensuring the pairing of these components can withstand the expected power of the MTRT. The belt and sprocket assembly is shown in the following figure, FIGURE 4-32.

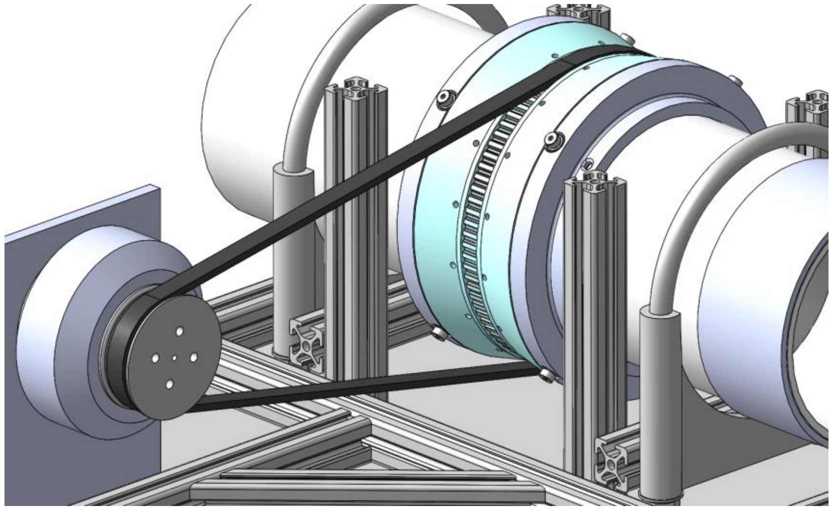

FIGURE 4-32: Belt drive in SOLIDWORKS assembly

The small sprocket and belt parameters drive the rated power of the system [45]. The following table describes the belt and sprocket parameters and the rated load; see TABLE 4-6.

TABLE 4-6: Belt drive analysis

Parameter	Value
Belt Description	Gates PowerGrip XL 310xL037
Sprocket Description	30XL (30 teeth, 1.91 in diameter)
Outer Rotor Description	85XL (85 teeth, 5.28 in diameter)
Expected Low Speed	2494 RPM (261 rad/sec)
Expected High Speed	7066 RPM
Rated Power	1.06 HP (790 W) [45]

From the manufactures design manual, [45], the maximum load at the expected speeds is 790 W which is much higher than the expected load of the powerplant. The selected components will be sufficient for the MTRT prototype.

The bearing analysis is necessary to ensure the bearings can withstand the expected radial loads and rotational speeds. The following table describes the bearing parameters and the rated values; see TABLE 4-7.

TABLE 4-7: Bearing analysis

Parameter	Value
Bearing Description	R2-5-2Z Shielded Stainless Steel Ball Bearing
Radial Load Capacity	120 lbs.
Maximum Expected Speed	33,922 RPM
Maximum Rated Speed	71,000 RPM

The configuration of the bearings on the inner and outer rotor makes for a complicated load. Because of the permanent magnet coupling theoretically balancing in the axial and radial position, there should be little radial load on the bearings. This is likely not going to occur in practice, however, the maximum radial load of 120 lbs. with a total of 16 bearings per rotor should suffice in the prototype testing. The expected rotational speed of the bearings is sufficiently under the maximum rated speed of the selected bearing.

4.3.5 Conclusion

The mechanical analysis for the prototype MTRT allowed for the assurance that the prototype will not fail mechanically during testing. The results generated were preliminary but sufficient to move the development forward into manufacturing and testing. Further exploration into bearing friction and actual radial load should be included in future work. Optimization of the bearing design has major implications for the maintenance and efficiency of the hydropower plant. The goal with moving the bearing design forward is to reduce bearing lubrication necessity and reduce friction forces during rotation. The bearing seals are also of concern and with the further development of the MTRT; different bearing technologies should be considered to reduce or eliminate the need for bearing lubrication and sealing. It is recommended for scaling up the concept that a more thorough analysis is completed with a better understanding of the expected loads on the system. In the implementation of the system, it is recommended that the standard IEC 62006 be reviewed and used for testing to meet the international standard on small hydroelectric installations.

CHAPTER 5: PROTOTYPE TESTING

The prototype testing consisted of field testing and laboratory testing. The purpose of the testing was to empirically determine the effectiveness of the MTRT hydropower plant. The testing completed for this thesis project allows for design issues to be identified so that a more optimized system can be achieved in the future continuation of this research. The success of this device requires continuous improvements to attract customers to implement this device.

5.1 Completed Prototype

The prototype MTRT device was assembled with components manufactured in the facilities of UNC Charlotte and purchased components that are commercially available. With the use of 3D printing, high complexity parts necessary in the system were able to be manufactured and installed in less than a day. The completely assembled prototype MTRT hydropower plant is shown in the following figure, FIGURE 5-1.

FIGURE 5-1: Assembled MTRT Prototype

The prototype shown in FIGURE 5-1 includes the permanent magnet generator that was selected for the prototype test. This generator is a re-purposed ultra-efficient RC helicopter motor produced by T-Motor. The generator has 3 phase stator coils and a permanent magnet outer rotor. To covert the “wild AC” output into a useful DC voltage a 3 phase diode rectifier is used (SQL 100A). This DC voltage allows for easier loading of the MTRT with the controlled dump load.

5.2 Field Test

5.2.1 Test Method

The field test involves running water through the hydropower plant to test the function of the MTRT. This test was completed at Appalachian State University at the micro hydro test facility in the Sustainable Technology and Built Environment department. The test facility provides approximately 1000 gallons of supply at 28 psi or 64.5 feet of head. The supply is fed through a 2 inch HDPE penstock pipe from the top of a hill on the Appalachian State University campus. This system in representative of a typical micro hydropower set-up with the exception the 2 inch to 4 inch expansion that is required to connect the prototype MTRT to the existing penstock. Ideally, the penstock would be 4 inches to reduce the loss in the expansion as well as the friction loss in the smaller diameter penstock from the higher velocity due to continuity. The set-up of the MTRT hydropower plant is shown in the following figure, FIGURE 5-2.

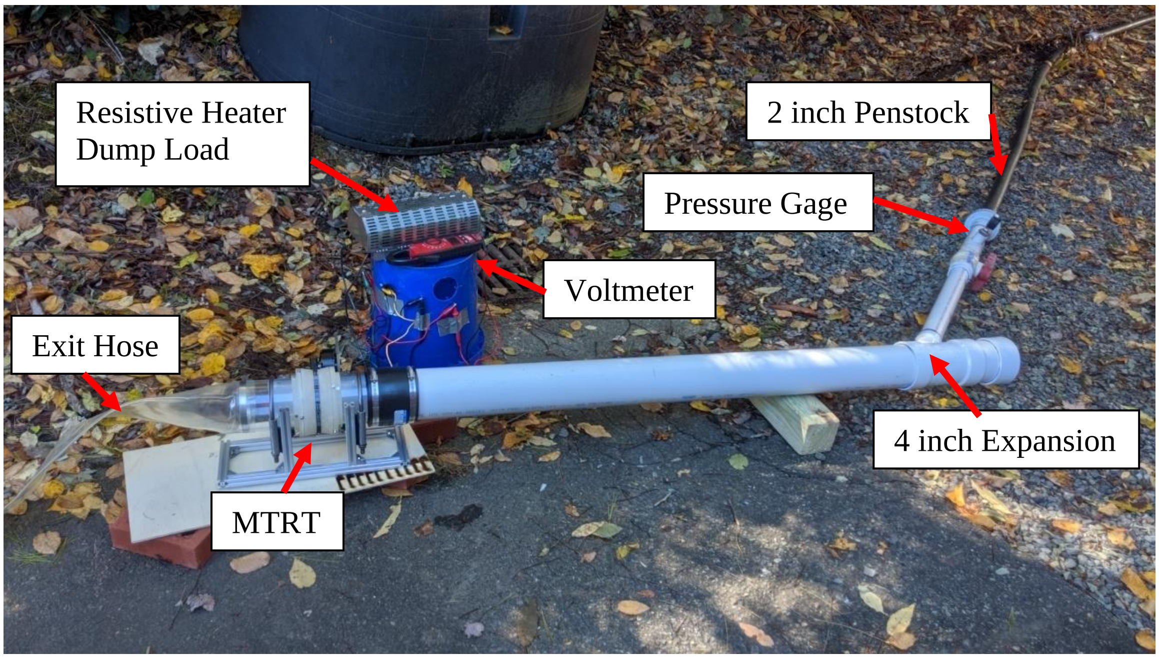

FIGURE 5-2: Field test set-up of MTRT hydropower plant

As shown in FIGURE 5-2, the test site includes all the necessary components for testing the MTRT. Because the penstock is 2 inches and the MTRT is 4 inches, an expansion wye had to be used to couple the MTRT with the penstock. To complete the circuit of the generator, a dump load was used to expel the energy generated by the MTRT. The dump load has a resistance of approximately 0.375 ohms. With the voltmeter, the power output of the generator can be established using ohms law.

5.2.2 Results

As the penstock valve was opened and water started flowing through the system the pressure on the gage dropped to 0 psi. This equates to a theoretical maximum fluid velocity of approximately 66 ft/s (20 m/s) in the 2 inch penstock. Considering the frictional losses in the tank exit (~5 ft of head), penstock (~20 ft of head), the wye expansion (~2 ft of head) and the MTRT , and the pipe diameter increase to 4 inches, the expected velocity is in the 4 inch pipe is approximately 11.48 ft/s (3.5 m/s) [46]. This value is greater than the estimation of the 1000 gallon tank draining through the system in approximately 12 minutes. This equates to a volumetric flow rate of 83 GPM and a fluid velocity in the 4 inch pipe of 2 ft/s (0.6 m/s). The difference in these values can be attributed to the losses in the MTRT and the other losses in the system that were unaccounted for. Due to the very low flow speed and frictional forces caused by the bearings in the system the turbine did not rotate during testing. After removing half of the bearings (8/16 per rotor remaining) and removing 75% of the magnets (4/16 per rotor remaining) the turbine rotated much more freely in the conduit. After running a second test, the turbine still did not rotate until the belt was removed. The torque applied by the generator connected to the dump load was greater than the torque that the turbine could produce so rotation was prevented. Once the belt was removed, the turbine spun at high speeds but did not produce electricity. The turbine spun at speeds estimated between 400 to 600 RPM with a strobe light tachometer. The generator is advertised as 80 RPM/Volt which means at the high speed of 400 to 600 RPM the motor would be producing 66.7 to 150 Watts which is much higher than the maximum potential of the water flow (~ 4 W). Future testing will use a variable resistance dump load so the generator torque can be reduced, and power can be produced. Also, future testing will require a higher available flow rate to achieve the necessary speeds to drive the turbine.

During the testing it was observed that the water flow through the turbine caused a large vortex to form downstream of the turbine. This large vortex lowers the efficiency so there should be consideration in the guide vane design to reduce the size of this vortex. This will most likely involve the use of fins on the inlet and outlet guide vanes. CFD simulation should be used to optimize the geometry for specific flow conditions.

5.3 Laboratory Test

The laboratory test determined the efficiency of the magnetic transmission and the generator of the hydropower plant. The laboratory test ignored the effect of fluid through the turbine and will focus on the performance of the other components in the path of energy conversion.

5.3.1 Test Method

The input power to the system is an electric servo motor with controllable speed and measured torque. The output power of the test is measure using the voltage of the DC rectifier connected to the generator and to a varying resistance dump load. Using National Instruments' hardware and software the speed and torque of the servo and the voltage out of the rectifier will be acquired and recorded for efficiency and other performance calculations. The test set-up is shown in the following figure, FIGURE 5-3.

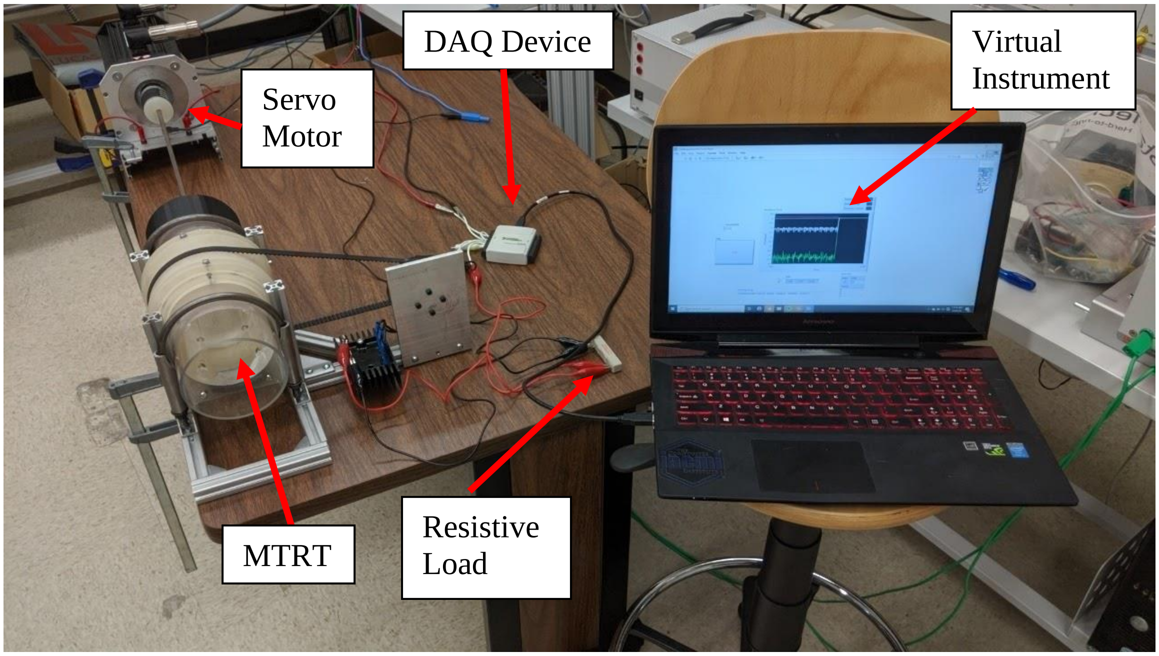

FIGURE 5-3: Laboratory MTRT Powerplant Test Set-up

5.3.2 Results

The efficiency and power output of the system was measured for the resistive load resistances of 1.5, 2.9. 5.4 and 10.2 ohms. The speed of the servo was increased up to 200 RPM and then decreased back to 0 RPM while the data acquisition device and software was recorded at 10 samples per second. The following figure shows the results of the power output of the generator and the efficiency of the magnetic transmission, mechanical components and electrical components within the system; see FIGURE 5-4.

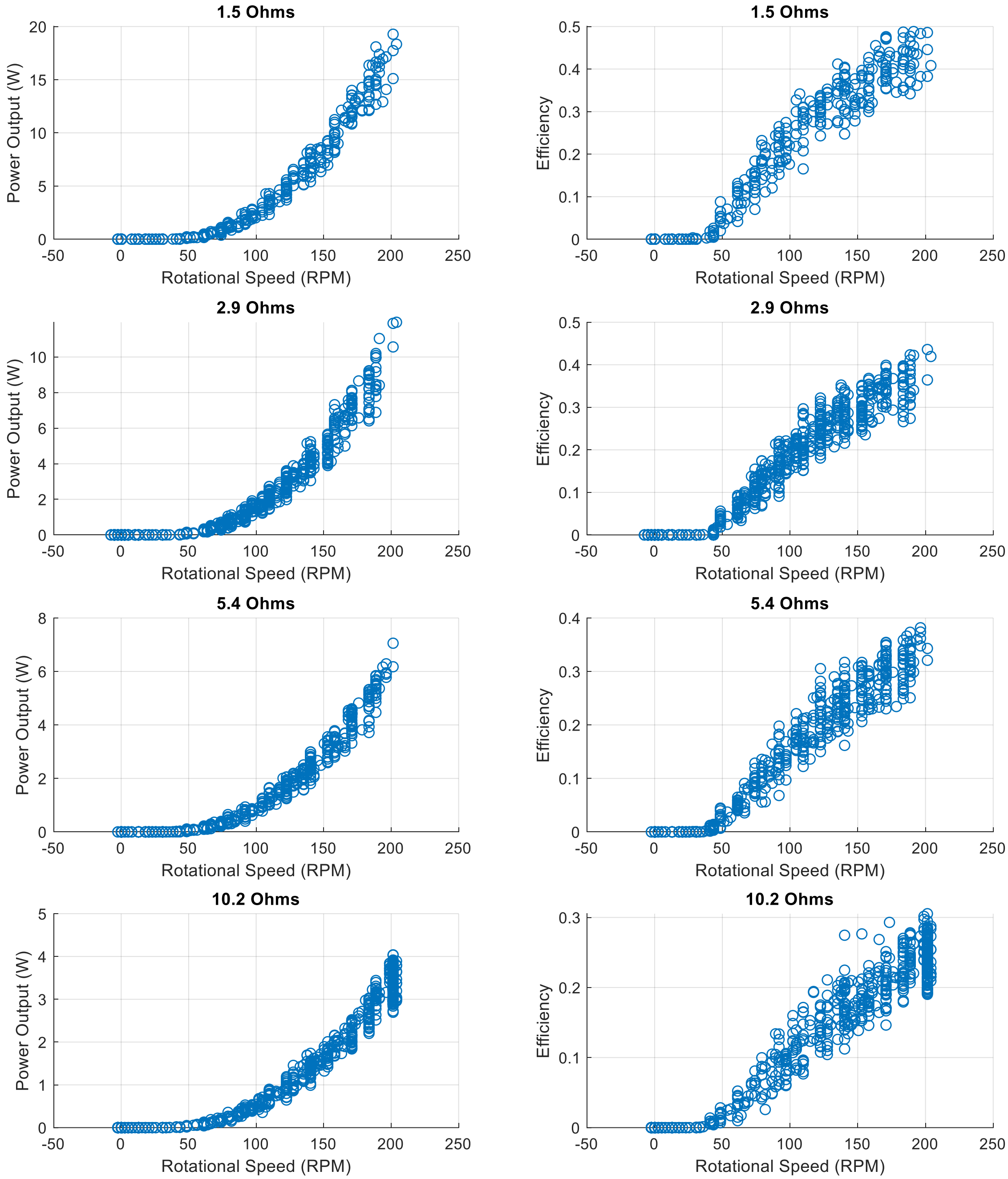

FIGURE 5-4: Power (left) and efficiency (right) raw data at varying rotational speeds and load resistances

It is observable in FIGURE 5-4 that the lower resistance loads produced more power at higher efficiencies. It is also observable that there is a significant amount of variation in the output power and efficiency causing a cloud of data points rather than a line. This is likely due to the varying frictional load in the mechanical components of the MTRT and the permanent magnet generator used in testing. It is not suspected to be electrical noise in the data acquisition system because noise levels in the electric signal were less than 0.005 V which equates to 5 RPM, 0.005 Nm and 0.005 V from the generator. These values are significantly less than the variations seen in the recorded data. The comparison of power output and efficiency depending on the resistive dump load is shown in the following figure, FIGURE 5-5.

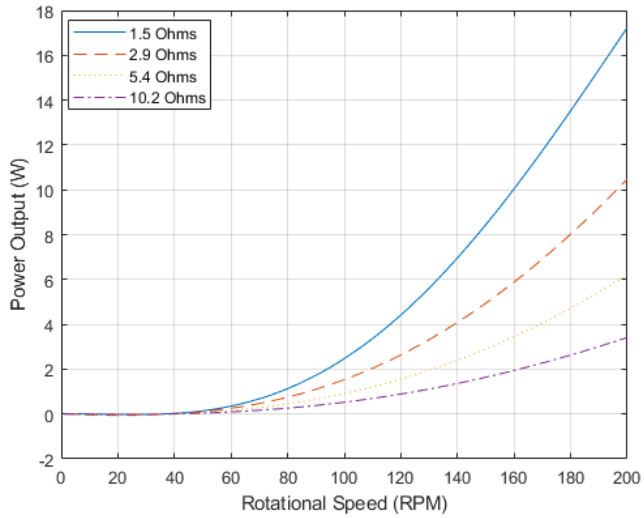

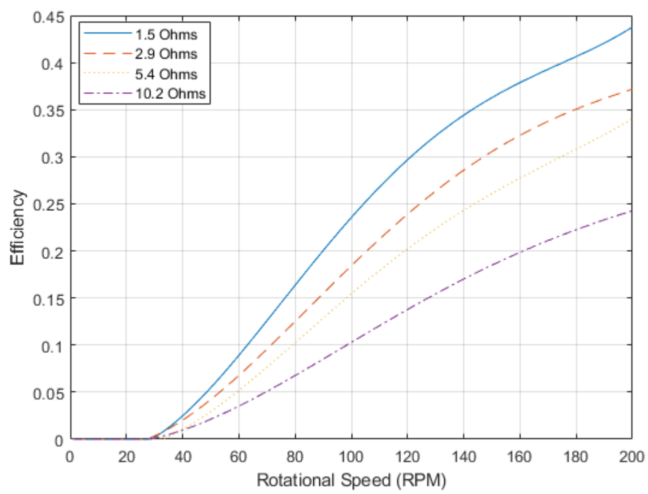

FIGURE 5-5: Power output and efficiency with respect to roational velocity and resisitve load.

FIGURE 5-5 was created with MATLAB using a 4th order polynomial curve fit of the data acquired during testing. The efficiency results were adjusted so negative values were not included in the results. From FIGURE 5-4 and FIGURE 5-5, it can be observed that the power output and efficiency stagnate at zero until the rotational velocity exceeds approximately 30 RPM. This is likely caused by the generator operating at very low speeds and not producing a voltage and also because losses in the system being equal to the input power at low speeds. It can be observed that the resistive load was inversely related to power output and efficiency. It should be noted that the resistive load values are not equally spaced. This is due to the inventory of power resistors used in testing not being equally spaced.

The laboratory testing provided useful insight of the operation of the MTRT hydropower plant with the exception of the hydrodynamic interaction. Quantifying the efficiency of the remaining components in the energy conversion path allows for this design to be compared to other designs in the past and future. Although the efficiency of the prototype was below 50%, the MTRT was successful in generating useful DC energy. Optimizations in future work would allow the MTRT to be an effective in-conduit hydropower plant.

CHAPTER 6: CONCLUSION

In the development of the MTRT hydropower plant, the analysis and the prototype testing arrived at the following conclusions. Through the computational fluid dynamics analysis, the structural loads that were being applied to the turbine were calculated and transferred to the mechanical analysis where it was found that the turbine can withstand the expected hydrodynamic loads. The magnetostatic analysis determined the peak torque of the magnetic transmission for the device. It was determined that the designed parts in the energy conversion path could withstand the expected loads without failing. It was also determined that the magnetic transmission, as originally designed, greatly exceed the maximum torque of the turbine in flowing water. Because of this, the quantity of permanent magnets in the transmission was reduced for testing. The design was successfully validated with standard procedures in CFD, magnetostatic and structural analysis with finite element simulation.

From the prototype testing, it was determined that the MTRT hydropower plant was successfully able to transfer the energy from inside the conduit to outside the conduit with the use of the magnetic transmission. This allowed for isolation between inside and outside the pipe without a mechanical seal. It was also determined that the in-conduit design allowed for the hydropower plant to be easily installed by a one or two-person team in under 10 minutes. The modular turbine component also allowed for the easy customization of the turbine depending on the site-specific flow characteristics. Also, the simple mechanical designed allowed for very quick disassembly and modification in-field.

Due to the early design stage of the device, the efficiency and power output of the prototype was low but there is potential to increase these values. Advancements in the fluid mechanics driven design of the penstock, turbine and draft tube could greatly increase these values. Also, the improved design of the bearing system for rotating the turbine inside the conduit would allow for higher power output and efficiency.

The development and testing of the MTRT prototype hydropower plant allows for the comparison of the technology with the similar technologies developed. The following table compares the existing technologies that are described in the literature review in section 1.3.1; see TABLE 6-1.

TABLE 6-1: Comparison of Similar In-Conduit Hydropower Plants with MTRT

	 Nustreem [11]	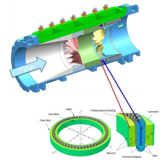 Rapidly Deployable… [12]	 LucidPipe [13]	 MTRT
Rated Power	75 – 250 kW	70 – 700 kW **	18 -100 kW	< 10 W ^^
Commercialized	Yes	No	Yes	No
Includes Seal	Yes	No	Yes	No
Modular	Yes	No	No	Yes
High Efficiency (90% +)	Yes	Yes	No	No
Controlled Output Power	Yes	Yes	No	No
Mechanical Overload Protection	No	No	No	Yes

** - Output power specified in scalability study
^^ - Estimate at current point in development

In TABLE 6-1, it can be observed that the MTRT is less developed than the similar technologies but the major benefits are the seal-free transmission, the modularity and the mechanical overload protection from the magnetic transmission. The magnetic transmission eliminates the need for a seal that requires leakage to be cooled and wears with time and requires service. Another benefit is that the magnetic transmission has the ability to slip poles like a clutch and protect the load carrying components from impact loads on the turbine from debris and water surges.

The use of rare-earth permanent magnets in devices is high risk because of uncertainties in the industry. Neodymium permanent magnets are usually an imported product which lends the cost to fluctuations caused by international trade laws and tariffs. However, the improvement of the design could allow for lower cost in permanent magnets. This is because the initial magnetic design was capable of much greater torque transfer than what is necessary. The device could be lower cost and remain functional if the magnetic mass was decreased and cheaper magnetic materials other than neodymium were used. Also, the high forces associated with the permanent magnets caused increase friction between the inner and outer rotors, and the pipe. If the magnets were moved further apart radially, the peak torque transmission would be reduced to a more suitable value and the magnetic forces causing friction would be reduced. Lowering the peak value of torque transmission has implications in mechanical overload protection. The ability of the magnetic transmission to slip poles and prevent overload is very advantageous for increasing the reliability of the device.

The future work for the improvement of the MTRT hydropower plant can be summarized as follows:

- Optimize design for higher output power, higher efficiency, greater pressure reduction and lower cost to manufacture
    - Improved bearing design
    - Improved turbine design
    - Larger pipe diameters, heads and flow rates
    - Increased pressure-drop across turbine
    - Improved permanent magnet configuration

- Design a full hydropower solution for micro hydropower. Buyers want a turn-key package that includes intake, penstock, hydropower plant and river return.
- Design database of turbine, penstock and draft tube geometries for specific flow parameters to allow for.
- Consider other applications for the seal-free transmission of mechanical energy
    - Medical and sterile fluid pumps
    - Impellers for watercraft propulsion
    - Pumping of volatile fluids requiring complete isolation from atmosphere

In conclusion, the research and development behind the MTRT was successful in creating a new type of hydropower plant that is installed in less than 10 minutes, disassembled and reassembled in less than 10 minutes, simple enough for a single person to install, capable of transmitting mechanical energy with no seal required and capable of slipping poles for mechanical overload protection. The combination of these features in a hydropower plant is novel to hydropower and is contributing to the progress towards more economically viable designs which require increased robustness and low maintenance requirements. The development of the MTRT hydropower plant still requires a considerable amount of work to be commercially ready, however, this thesis has built a strong engineering foundation and has demonstrated the high potential of this technology.

REFERENCES

[1] "Monthly Energy Review – October 2018," *US Energy Inf. Adm.*, vol. October 2018, p. 272, 2018.

[2] "Role of Dams," *International Commission on Large Dams*, 2015. [Online]. Available: http://www.icold-cigb.org/GB/Dams/role_of_dams.asp. [Accessed: 31-Oct-2018].

[3] E. R. Ekstrand and J. Loomis, "Incorporating respondent uncertainty when estimating willingness to pay for protecting critical habitat for threatened and endangered fish," *Water Resour. Res.*, vol. 34, no. 11, pp. 3149–3155, Nov. 1998.

[4] M. Bellis, "The History of the Water Wheel," *ThoughtCo.*, 24-Nov-2019. [Online]. Available: https://www.thoughtco.com/history-of-waterwheel-4077881. [Accessed: 25-Nov-2019].

[5] C. Cleveland, "China's Monster Three Gorges Dam Is About To Slow The Rotation Of The Earth," *Business Insider*. [Online]. Available: https://www.businessinsider.com/chinas-three-gorges-dam-really-will-slow-the-earths-rotation-2010-6. [Accessed: 25-Nov-2019].

[6] S. N. Wilson, "Turbine Main Shaft Seal Leakage: Understanding the Problem," *Hydro Rev.*, vol. 18, no. 5, Nov. 2010.

[7] O. Paish, "Small hydro power: technology and current status," *Renew. Sustain. Energy Rev.*, vol. 6, no. 6, pp. 537–556, Dec. 2002.

[8] H. M. Ramos, M. Simão, and A. Borga, "Experiments and CFD Analyses for a New Reaction Microhydro Propeller with Five Blades," *J. Energy Eng.*, vol. 139, no. 2, pp. 109–117, Jun. 2013.

[9] A. Date and A. Akbarzadeh, “Design and cost analysis of low head simple reaction hydro turbine for remote area power supply,” *Renew. Energy*, vol. 34, no. 2, pp. 409–415, Feb. 2009.

[10] G. Lucian, “The Influence of Factors Acting on the Friction Power Losses in Mechanical Seals with Sliding Rings,” *J. Mar. Technol. Environ.*, vol. 1, pp. 51–56, Apr. 2011.

[11] “NUSTREEM,” *Nustreem Technology A modernized and modular Dual-Regulated Kaplan Design.* [Online]. Available: http://nustreem.com/technology/. [Accessed: 01-Aug-2019].

[12] A. Fontaine, N. Jaffa, T. Palmer, and J. Banks, “Rapidly Deployable Advanced Integrated Low Head Hydropower Turbine Prototype,” presented at the Water Power Technologies Office Peer Review, Penn State University Applied Research Lab, 13-Feb-2017.

[13] LucidEnergy, “The LucidPipe™ Power System (LPS),” *Lucid Energy*. [Online]. Available: http://lucidenergy.com/how-it-works/. [Accessed: 02-Nov-2018].

[14] D. R. Giosio, A. D. Henderson, J. M. Walker, P. A. Brandner, J. E. Sargison, and P. Gautam, “Design and performance evaluation of a pump-as-turbine micro-hydro test facility with incorporated inlet flow control,” *Renew. Energy*, vol. 78, pp. 1–6, Jun. 2015.

[15] Z. Qian, F. Wang, Z. Guo, and J. Lu, “Performance evaluation of an axial-flow pump with adjustable guide vanes in turbine mode,” *Renew. Energy*, vol. 99, pp. 1146–1152, Dec. 2016.

[16] R. K. Saket, R. C. Bansal, and K. S. A. Kumar, “Reliability Evaluation of Micro Hydro-Photo-Voltaic Hybrid Power Generation Using Municipal Waste Water,” *GMSARN Int. J.*, vol. 1, pp. 13–20, 2007.

[17] O. de la Torre, D. Moore, D. Gavigan, and J. Goggins, “Accelerated life testing study of a novel tidal turbine blade attachment,” *Int. J. Fatigue*, vol. 114, pp. 226–237, Sep. 2018.

[18] J. L. Kueny, T. Lalande, J. J. Herou, and L. Terme, “Optimal design of a tidal turbine,” *IOP Conf. Ser. Earth Environ. Sci.*, vol. 15, no. 4, p. 042038, Nov. 2012.

[19] K. K. Uppalapati, J. Z. Bird, D. Jia, J. Garner, and A. Zhou, “Performance of a magnetic gear using ferrite magnets for low speed ocean power generation,” in *2012 IEEE Energy Conversion Congress and Exposition (ECCE)*, 2012, pp. 3348–3355.

[20] P. O. Rasmussen, T. O. Andersen, F. T. Joergensen, and O. Nielsen, “Development of a high performance magnetic gear,” in *38th IAS Annual Meeting on Conference Record of the Industry Applications Conference, 2003.*, 2003, vol. 3, pp. 1696–1702 vol.3.

[21] A. H. Neuland, “Apparatus for transmitting power,” US1171351A, 08-Feb-1916.

[22] K. Atallah, S. D. Calverley, and D. Howe, “Design, analysis and realisation of a high-performance magnetic gear,” *IEE Proc. - Electr. Power Appl.*, vol. 151, no. 2, pp. 135–143, Mar. 2004.

[23] K. Li, “An Investigation into the Torque Capabilities of High Gear Ratio Magnetic Gearboxes,” University of North Carolina at Charlotte.

[24] L. Jing, L. Liu, M. Xiong, and D. Feng, “Parameters Analysis and Optimization Design for a Concentric Magnetic Gear Based on Sinusoidal Magnetizations,” *IEEE Trans. Appl. Supercond.*, vol. 24, no. 5, pp. 1–5, Oct. 2014.

[25] K. Davey *et al.*, “Rotating Cylinder Planetary Gear Motor,” *IEEE Trans. Ind. Appl.*, vol. 52, no. 3, pp. 2253–2260, May 2016.

[26] W. N. Fu and L. Li, “Optimal Design of Magnetic Gears With a General Pattern of Permanent Magnet Arrangement,” *IEEE Trans. Appl. Supercond.*, vol. 26, no. 7, pp. 1–5, Oct. 2016.

[27] E.-J. Park, S.-J. Kim, and Y.-J. Kim, “Optimum design of salient magnetic gear with novel pole piece by central composite design,” *Int. J. Appl. Electromagn. Mech.*, vol. 54, no. 2, pp. 281–288, May 2017.

[28] D. Som *et al.*, “Analysis and Testing of a Coaxial Magnetic Gearbox With Flux Concentration Halbach Rotors,” *IEEE Trans. Magn.*, vol. 53, no. 11, pp. 1–6, Nov. 2017.

[29] J. F. Charpentier and G. Lemarquand, “Calculation of ironless permanent magnet couplings using semi-numerical magnetic pole theory method,” *COMPEL - Int. J. Comput. Math. Electr. Electron. Eng.*, vol. 20, no. 1, pp. 72–89, Mar. 2001.

[30] A. H. Elbatran, O. B. Yaakob, Y. M. Ahmed, and H. M. Shabara, “Operation, performance and economic analysis of low head micro-hydropower turbines for rural and remote areas: A review,” *Renew. Sustain. Energy Rev.*, vol. 43, pp. 40–50, Mar. 2015.

[31] D. A. Zema, A. Nicotra, V. Tamburino, and S. M. Zimbone, "A simple method to evaluate the technical and economic feasibility of micro hydro power plants in existing irrigation systems," *Renew. Energy*, vol. 85, pp. 498–506, Jan. 2016.

[32] K. Thorburn and M. Leijon, "Case study of upgrading potential for a small hydro power station," *Renew. Energy*, vol. 30, no. 7, pp. 1091–1099, Jun. 2005.

[33] L. Kosnik, "The potential of water power in the fight against global warming in the US," *Energy Policy*, vol. 36, no. 9, pp. 3252–3265, Sep. 2008.

[34] S. Kelly-Richards, N. Silber-Coats, A. Crootof, D. Tecklin, and C. Bauer, "Governing the transition to renewable energy: A review of impacts and policy issues in the small hydropower boom," *Energy Policy*, vol. 101, pp. 251–264, Feb. 2017.

[35] W. K. George, "Lectures in Turbulence for the 21st Century." Imperial College of London, 16-Jan-2013.

[36] F. R. Menter, "Zonal Two Equation k·co Turbulence Models for Aerodynamic Flows.," *AIAA*, vol. 24th Fluid Dynamics Conference, p. 22, Jul. 1993.

[37] D. Meeker, "Finite Element Method Magnetics," *Finite Element Method Magnetics*, 23-Jun-2019. [Online]. Available: http://www.femm.info/wiki/HomePage. [Accessed: 25-Sep-2019].

[38] D. Meeker, "Finite Element Method Magnetics User's Manual." 30-Jan-2018.

[39] G. H. Jang, J. W. Yoon, N. Y. Park, and S. M. Jang, "Torque and unbalanced magnetic force in a rotational unsymmetric brushless DC motors," *IEEE Trans. Magn.*, vol. 32, no. 5, pp. 5157–5159, Sep. 1996.

[40] A. Armenakas, *Advanced Mechanics of Materials and Applied Elasticity*, 1st ed. Boca Raton: CRC Press, 2016.

[41] Proto-Pasta, “Iron-filled Metal Composite PLA – ProtoPlant, makers of Proto-pasta,” *products*. [Online]. Available: https://www.proto-pasta.com/products/magnetic-iron-pla. [Accessed: 22-Aug-2019].

[42] K&J Magnetics, “K&J Magnetics - Physical and Mechanical Characteristics,” *Specifications*. [Online]. Available: https://www.kjmagnetics.com/specs.asp. [Accessed: 04-Oct-2019].

[43] “VisiJet M3 Crystal Advanced Plastics Technical Specifications.” 3D Systems, 2019.

[44] Y. Nishi, T. Inagaki, K. Okubo, and N. Kikuchi, “Study on an Axial Flow Hydraulic Turbine with Collection Device,” *International Journal of Rotating Machinery*, 2014. [Online]. Available: https://www.hindawi.com/journals/ijrm/2014/308058/. [Accessed: 24-Sep-2019].

[45] “PowerGrip Drive Design Manual.” Gates Corporation, 2014.

[46] B. R. Munson, *Fundamentals of fluid mechanics*, 7th ed. Wiley, 1990.

APPENDIX: FEMM TORQUE ANALYSIS MATLAB SCRIPT

```
%Torque Analysis

clear
clc

openfemm %opens the femm software gui
opendocument('FEMM_Final_air.FEM') %opens femm document that was
already created
mi_probdef(0,'inches','planar',.00000001,1.5,30,0) %sets up femm
problem
pts = 200 %number of data points in simulation
tot_offset = 45 %total degree sweep in simulation
Torque=zeros(1,pts-1) %sets up torque matrix
deg_offset= [0:tot_offset/(pts-1):tot_offset] %degree offset for
simulation

for i=1:pts
mi_analyze %completes femm calculation
mi_loadsolution %loads results

%it is important to have the group of magnets/cage elements in group 1
(lines, points and blocks) to
%calculate torque and rotate
mo_groupselectblock(1) %selects the blocks associated with group 1
Torque(1,i) = mo_blockintegral(22) %calculates weighted torque with
stress tensor (22)
mi_selectgroup(1) %selects the group 1 elements
mi_moverotate(0,0,-tot_offset/pts) %rotates the rotor about point 0,0


end


plot(deg_offset,Torque)
Torque = Torque'
deg_offset = deg_offset'

%creates txt file with results in MATLAB folder with date and time (be
sure to note somewhere what the simulation description is
T = table(Torque,deg_offset)
t = datetime('now')
filename = datestr(t,'mm-dd-yyyy HH-MM')
fileID = fopen(filename,'w');
writetable(T,filename)
```